

# TWO SAMPLE INFERENCE FOR POPULATIONS OF GRAPHICAL MODELS WITH APPLICATIONS TO FUNCTIONAL CONNECTIVITY

BY MANJARI NARAYAN<sup>\*</sup>, GENEVERA I. ALLEN<sup>\*,†,‡</sup> AND STEFFIE N. TOMSON<sup>§</sup>

*Dept. of Electrical Engineering<sup>\*</sup> & Dept. of Statistics, Rice University<sup>†</sup>,  
Dept. of Pediatrics-Neurology, Baylor College of Medicine & Jan and Dan Duncan Neurological  
Research Institute, Texas Children's Hospital<sup>‡</sup>, Dept. of Psychiatry, UCLA<sup>§</sup>*

*Abstract* Gaussian Graphical Models (GGM) are popularly used in neuroimaging studies based on fMRI, EEG or MEG to estimate functional connectivity, or relationships between remote brain regions. In multi-subject studies, scientists seek to identify the functional brain connections that are different between two groups of subjects, i.e. connections present in a diseased group but absent in controls or vice versa. This amounts to conducting two-sample large scale inference over network edges post graphical model selection, a novel problem we call Population Post Selection Inference. Current approaches to this problem include estimating a network for each subject, and then assuming the subject networks are fixed, conducting two-sample inference for each edge. These approaches, however, fail to account for the variability associated with estimating each subject's graph, thus resulting in high numbers of false positives and low statistical power. By using resampling and random penalization to estimate the post selection variability together with proper random effects test statistics, we develop a new procedure we call  $R^3$  that solves these problems. Through simulation studies we show that  $R^3$  offers major improvements over current approaches in terms of error control and statistical power. We apply our method to identify functional connections present or absent in autistic subjects using the ABIDE multi-subject fMRI study.

**1. Introduction.** Functional connectivity seeks to find statistical dependencies between neural activity in different parts of the brain (Smith, 2012; Smith et al., 2013). It has been studied at a systems or whole brain level using noninvasive imaging techniques such as functional MRI (fMRI), EEG and MEG, or using more invasive techniques at the micro level such as electrophysiology or ECoG. Whole brain functional connectivity has become especially popular to study in resting state fMRI where subjects lie in the scanner passively at rest (Smith, 2012). For this data, connectivity is typically modeled as a network with functionally or anatomically derived brain regions as nodes and connections as undirected edges (Bullmore and Sporns, 2009). In this paper, we are particularly interested in studying multi-subject functional connectivity for resting-state fMRI data; the statistical challenges we outline and methods we develop, however, are applicable to functional connectivity in many neuroimaging modalities.

Many have sought to use functional connectivity and more broadly connectomics to better understand neurological conditions and diseases. Specifically, we seek to address the question - How are functional connections different in a group of diseased subjects than in healthy controls? - by conducting inference across a population of brain networks. This

---

*MSC 2010 subject classifications:* functional connectivity, neuroimaging, graphical models, random effects, post selection inference, population post selection inference

question has been well studied in the neuroimaging literature; see (Milham, 2012; Craddock et al., 2013) for detailed reviews. Indeed, neuroscientists have used these techniques to find connectivity biomarkers for diseases such as Alzheimer’s and clinical depression (Tam et al., 2014; Tao et al., 2013). However, we will show that these widely used methods suffer from major statistical flaws that can result in high error rates. Understanding and solving these flaws presents us with a new type of statistical problem, something that we will term *Population Post Selection Inference (popPSI)*, that has been previously unaddressed in the statistics literature. Thus in this paper, we have three major objectives: (1) To introduce this completely new problem that arises in population functional connectivity to the statistical community; (2) To discuss the open statistical challenges that arise with this problem and diagnosis problems associated with the currently used methods in neuroimaging; and (3) To introduce a new statistical method that partially solves these problems, leading to much improved performance in terms of statistical power and error control.

1.1. *Current Standard in Neuroimaging.* Before proceeding to define our problem, we pause to understand current approaches in the neuroimaging literature to conducting inference across a population of brain networks. The current standard as described in (Zalesky, Fornito and Bullmore, 2010; Bullmore and Sporns, 2009; Zalesky et al., 2012; Meda et al., 2012; Palaniyappan et al., 2013) follows three main steps after a pre-processing step to format the data:

- Step 0. Parcellate data for each subject.
- Step 1. Estimate a brain network for each subject.
- Step 2. Aggregate graph metrics for each subject.
- Step 3. Conduct two-sample inference on the graph metrics across subjects.

Henceforth, we will refer to this approach as the standard method. We discuss each of these steps in further detail.

Resting-state functional MRI (fMRI) data is acquired as three-dimensional volumes ( $\approx 10,000 - 100,000$  voxels) over time ( $\approx 50 - 500$  time points captured every 2-3 seconds) as each subject lies in the scanner at rest. Studying functional brain networks at the voxel level is not desirable as most connections would be due to close spatial proximity and hence subject to physiological confounds (Craddock et al., 2013; Turk-Browne, 2013). Thus, voxel level connections are difficult to interpret. As a result, most study brain networks where each node is an anatomical or functionally derived brain region. After standard fMRI pre-processing which includes registering each subject’s volume to a common template (Beckmann, Jenkinson and Smith, 2003), each subject’s brain scan is parcellated by mapping voxels to anatomical regions (e.g. AAL, Talarach, or Harvard-Oxford atlas (Fischl et al., 2004)), or functionally derived regions (Power et al., 2011). The time series of the voxels are then averaged within each region, yielding a matrix,  $\mathbf{X}_{p \times T}$ , for  $p$  brain regions ( $\approx 90 - 500$ ) and  $T$  time points for each subject.

Given the parcellated fMRI data for each subject, Step 1 estimates a brain network connecting the  $p$  brain regions for each subject. While there are many statistical models that have been used to estimate brain networks (see (Craddock et al., 2013; Simpson et al., 2013a) for a thorough review), by far the most common is to use thresholded correlation matrices (Zalesky, Fornito and Bullmore, 2010; Bullmore and Sporns, 2009; Zalesky et al., 2012; Palaniyappan et al., 2013). However, thresholded partial correlations have also been employed as in a recent paper (Tao et al., 2013).

In Step 2, neuroimagers take the subject networks as fixed and study topological properties of these networks using techniques adapted from physics and computer science. These so-called “graph metrics” summarize certain properties of the networks such as degree, node centrality, participation coefficient, modularity, and efficiency among many others; see (Sporns, 2011) and the software (Rubinov and Sporns, 2010) for a complete list of commonly used topological metrics in neuroimaging.

Finally in Step 3, neuroimagers compare values of the graph metrics from Step 2 across the population of subjects using large-scale statistical inference. For two group populations (e.g. controls vs. diseased), this typically entails using standard two-sample test statistics such as a two-sample  $t$ -test for continuous graph metrics or a two-sample test for proportions for binary graph metrics. As many have noted the benefits of non-parametric procedures, most use permutation null distributions instead of asymptotic theoretical nulls (Zalesky, Fornito and Bullmore, 2010; Simpson et al., 2013b). Finally, as many of the graph metrics result in a statistic for each node of the network (i.e. the degree of each network node), neuroimagers correct for multiplicity, typically by controlling the false discovery rate (FDR) (Zalesky, Fornito and Bullmore, 2010). To summarize, the final inference step to test for differences in a single graph metric across two subject groups consists of three sub-steps - two-sample test statistics, permutation nulls, corrections for multiple testing (Zalesky, Fornito and Bullmore, 2010).

1.1.1. *Our Problem.* The above outline of population inference for functional connectivity is broad and is used for testing many types of graph metrics and with many types of statistical network models. In this paper, we wish to study this problem carefully and hence focus on a very specific statistical problem: Using Markov Networks and specifically Gaussian Graphical Models (GGMs) as the model for subject-level networks, we seek to test for the differential presence of a single network edge in one group of subjects. Thus, we assume that the observed multi-subject fMRI data,  $\mathbf{X}_{n \times p \times T}$  for  $n$  subjects,  $p$  brain regions, and  $T$  whitened time points, arises from the following model:

$$\begin{aligned} \text{Subject-Level: } & x_j^{(i)} \stackrel{iid}{\sim} N(0, (\Theta^{(i)})^{-1}) \quad \forall j = 1, \dots, T. \\ (1) \quad \text{Group-Level: } & Y_{k,l}^{(i)} = \mathbb{I}(\theta_{k,l}^{(i)} \neq 0) \sim \text{Bern}(\pi_{k,l}^g) \quad \forall i \in \mathcal{G}_g \text{ \& } \forall 1 \leq k < l \leq p. \end{aligned}$$

Here,  $\Theta_i$  is the  $p \times p$  sparse inverse covariance matrix for subject  $i$  with  $\theta_{k,l}$  denoting the  $k, l^{\text{th}}$  matrix element,  $g$  denotes group membership, and  $\pi_{k,l}^g$  denotes the group level probability of an edge at  $(k, l)$ . We assume that each subject follows a separate Gaussian graphical model (GGM), but that the support of each edge in the graph structure follows some group-level probability. Note that this permits each subject to have a potentially different brain network, an important attribute as we expect each subject to have a slightly different brain network. Given this population of GGMs, we seek to test for differential edge support between two groups of subjects, by testing the following hypothesis for each edge,  $(k, l)$ :

$$(2) \quad \mathcal{H}_0 : \pi_{(k,l)}^A = \pi_{(k,l)}^B \quad \text{vs.} \quad \mathcal{H}_1 : \pi_{(k,l)}^A \neq \pi_{(k,l)}^B.$$

This corresponds to asking whether a single functional connection in the brain network is more present in one group of subjects than the other. For example with autistic subjects (which we will study further in our case study in Section 5), we may hypothesize that autistic subjects will have fewer edges than healthy controls between the fusiform gyrus which is

responsible for facial cognition and other regions such as the occipital lobe associated with social cognition. Our ultimate goal is to develop an inferential procedure for testing (2) based on the model (1) that has high statistical power and controls or limits the false positives, either for testing a single edge or the false discovery rate (FDR) for testing many edges.

While the inference problem we study is a special case of the general framework employed in neuroimaging, it is nonetheless a new problem that has not been specifically addressed by the neuroimaging community. Several, however, have used Markov Networks and GGMs to study functional connectivity (Huang et al., 2010; Smith et al., 2011; Ryali et al., 2012); many others have used closely related partial correlations to model connectivity (Marrelec et al., 2006). These models offer several advantages for connectivity as they capture more direct functional connections compared to correlation-based networks, correspond to a coherent statistical model, and have been shown to be more robust to physiological constructs such as head motion (Yan et al., 2013). Also, while most conduct inference on graph metrics, several have proposed to test individual edges (Zalesky, Fornito and Bullmore, 2010; Varoquaux and Craddock, 2013; Lee, Shimojo and O'Doherty, 2014); moreover, several specific functional connections have been associated with clinical conditions (Bullmore, 2012; Tao et al., 2013). Finally, we note that testing edges in Markov Networks is more powerful than testing correlations as differential connections can be pinpointed to precise brain regions because of the conditional dependence relationships.

Our problem is also new from a statistical perspective, but related to several other problems in the statistical literature. For example, some have noted that testing for functional connections in a population is akin to testing for zero entries in the covariance or precision matrix (Ren et al., 2013). Others have proposed to test for differences between the elements of two covariances (Cai, Liu and Xia, 2013; Zhao, Cai and Li, 2014). When applied to functional connectivity, however, these inference procedures make the key assumption that all subjects share the same network model, an assumption that we do not make. Also, some have proposed methods to find network differences based on perturbations to random networks (Balachandran, Airolidi and Kolaczyk, 2013) or testing procedures for the stochastic block model (Vogelstein et al., 2013). Importantly, these classes of methods assume a model that generates the networks and not one that generates the observed subject-level data directly. Finally, many have sought to characterize differences in subject networks through estimation via multiple GGMs (Guo, Elizaveta Levina and Zhu, 2011; Danaher, Wang and Witten, 2011) instead of through direct inference as we propose.

1.2. *Population Post Selection Inference.* Our model, (1), is a two-level model, and there is a large body of statistical literature on estimation and inference for multi-level and random effects models; see (Searle, Casella and McCulloch, 2009) for an overview. Unfortunately, we will not be able to directly employ any of these classical estimates and inference procedures for our problem. To estimate the subject-level parameters,  $\Theta$ , corresponding to subject-level brain networks, we will need to use sparse graph selection techniques. This is necessary as first, we are testing the sparse support of  $\Theta$ ; additionally, we expect functional connectivity to be a sparse network; and finally, often the number of brain regions considered,  $p$ , is larger than the number of resting-state time points,  $T$ , thus necessitating regularized maximum likelihood estimation. By using a selection procedure to estimate the subject-level parameters, however, our parameter estimates no longer follow known distributions, negating the possibility of employing classical random effects methods.

Inference for multi-subject functional connectivity then gives rise to a completely new

class of challenging multi-level statistical inference problems. We term this new class of problems *Population Post Selection Inference (popPSI)* and define these as follows: PopPSI problems are two-level problems in which a variable selection procedure is used for parameter estimation at the subject-level and inference is to be conducted on parameters at the group level. In our case, the variable selection problem at level one corresponds to using graph selection to estimate the brain networks for each subject, and the inference problem at level two corresponds to testing for differential edge support between two groups of subjects. Indeed, any multi-subject inference problems for functional connectivity can be seen as popPSI problems.

We employ the name Population PSI to denote the close connection to Post Selection Inference (PSI) (Berk et al., 2013). A growing literature on PSI has focused on inference, including p-values and confidence intervals, for the coefficients of linear regression after selection via lasso-type estimators (Wasserman and Roeder, 2009; Zhang and Zhang, 2014; van de Geer, Bühlmann and Ritov, 2013; Javanmard and Montanari, 2013) others have discussed PSI for graph selection (Wasserman, Kolar and Rinaldo, 2013). This current PSI literature, however, has focused on conducting inference directly on the selected parameters in a single-level model. Our Population PSI problem, on the other hand, seeks to aggregate selected parameters across subjects and conduct inference between subject groups at the population level. This then, presents a new class of statistical problems that poses many new challenges.

In this paper, we focus on better understanding this new popPSI problem, especially our specific inference problem outlined in (2), and propose a novel methodological approach that offers dramatic improvements over the current standard in neuroimaging. In Section 2, we seek to understand the performance of the standard method in neuroimaging for our inference problem (2); namely, we show that the standard method has very high error rates with low statistical power. Investigating the standard method, we outline two challenges characteristic of our popPSI problem that are unaddressed by the standard method: two levels of network variability, Section 2.2, and biases resulting from graph selection errors, Section 2.3. In Section 3, we propose a novel method named  $R^3$  that uses resampling, random effects, and random penalization to address the first challenge and partially address the second challenge raised previously. Our new  $R^3$  method integrates the three steps of the standard approach into one procedure and by doing so offers substantial gains in statistical power and error control. We investigate our method, variations of our approach, and the standard method in extensive simulation studies in Section 4. In Section 5, we apply our method to the ABIDE multi-subject fMRI study to find functional connections that are associated with autism. We conclude with a discussion in Section 6. Also we note that while there are a plethora of open theoretical questions that arise with new popPSI problems and our specific problem, in this paper, we focus on building an intuition behind the challenges associated with these problems and propose a methodological solution; we save theoretical investigations for future work.

**2. Challenges of Population Post Selection Inference.** Our new Population PSI problem introduced in Section 1 will pose many challenges both methodologically and theoretically. We identify two challenges that are broadly characteristic of popPSI problems when conducting inference on multiple unobserved networks in high dimensions. In order to understand these challenges, we carefully examine the standard approach and highlight its shortcomings in the context of our particular inference problem, (2).

2.1. *Investigating the Standard Approach.* We begin by motivating the need for alternatives to the standard approach, outlined in Section 1.1, by studying this in the context of our model (1) and inference problem (2). Recall that the standard approach begins by estimating a graph structure independently for each subject; for our problem, this entails selection and estimation for Gaussian graphical models for which there are many well known procedures (Friedman, Hastie and Tibshirani, 2008; Meinshausen and Bühlmann, 2006). (We discuss these further for our particular problem in Section 3). Next, the standard method aggregates graph metrics for each subject which for our problem are the simple binary edge presence or absence indicators for each edge in the network. Finally, the standard approach conducts inference across subjects on the graph metrics; for our problem, this means testing for differences in the edge support across the two groups of subjects. For this, we can use a two-sample difference of proportions test for each edge  $(k, l)$ :  $T = \frac{\hat{\pi}^A - \hat{\pi}^B}{\sqrt{s_A^2 + s_B^2}}$ , where  $\hat{\pi}^A$  is the observed proportion of edge  $(k, l)$  in subject group  $A$ , and  $s_g^2 = \frac{1}{n_g} \hat{\pi}^g (1 - \hat{\pi}^g)$  is the usual estimate of the sample binomial variance. As previously mentioned, most use permutation testing to obtain p-values and correct for multiplicity by controlling the FDR; we do the same noting that as our test statistics are highly dependent due to the network structure, we use the Benjamini-Yekutieli procedure for dependent tests (Benjamini and Yekutieli, 2001).

To understand the performance of this standard method, we present a small preview of our simulation study discussed later in Section 4. Briefly, we assume that each subject graph in group  $A$  follows a small-world structure on  $p = 50$  nodes; in group  $B$ , there are in addition 150 differential edges, meaning that  $\pi_{(k,l)}^A = 1$  and  $\pi_{(k,l)}^B = 1$  for all differential edges,  $(k, l)$ . We generate data according to this model with  $T = 400$  time points and  $n_A = n_B = 20$  subjects in each group. Figure 1 illustrates the results of this standard approach as well as our new procedure,  $R^3$ , which we will introduce later in Section 3. Part (a) gives ROC curves for the number of false positives versus true positives as each sequential test is rejected; parts (b) and (c) give the adjacency confusion matrix illustrating where the true and false positive as well as false negative edges are detected in the graph structure.

Our motivating simulation shows that the standard approach performs terribly in terms of both error control and statistical power. While the magnitude of the poor performance of this approach may seem astonishing, the poor performance should come as no surprise: The inferential procedure (e.g. test statistics) of the standard approach assume a one-level model that would be appropriate when the subject graphs are fixed and known or directly observed quantities. When these subject networks are unobserved, however, and must be estimated from finite data, these one-level test statistics are incorrect for our two-level problem. Specifically for two-level problems, the variance of parameters estimated by incorrectly assuming a one-level models is underestimated. For our problem, the extra source of variability arises from the graph selection procedure; we discuss challenges associated with this subsequently in Section 2.2. Incorrect variance estimates, however, are not the only problem with the standard approach: A more subtle problem arises from the fact that the proclivities of graph selection procedures for the Gaussian graphical model lead to biased estimates of the edge proportions,  $\hat{\pi}^g$ . As discussed in Section 2.3 and seen in Fig 1, graph selection false positives and false negatives do not occur at random throughout the network structure, leading to biased group level estimates.

Also, it is important to note that the standard approach corresponding to a one-level problem would be appropriate if we were able to *perfectly* estimate the network structure for each subject as this is then the same as assuming the subject networks were directly observed. For

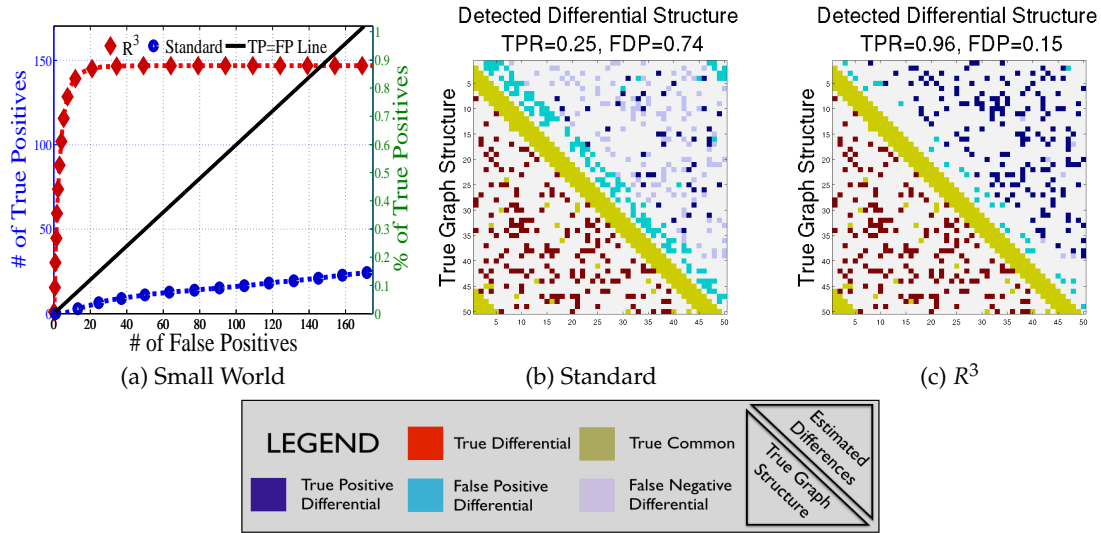


Figure 1: Motivating simulation study comparing the standard approach to our proposed procedure,  $R^3$ , in terms of (a) ROC curves for sequentially rejected tests, and confusion adjacency matrices along with observed true positive rate (TPR) and false discovery proportion (FDP) for (b) the standard method and (c) our approach. The standard method performs poorly in terms of both error control and statistical power.

typical fMRI data, however, this is unlikely to ever happen due to (i) the limited sample size,  $T$ , relative to  $p$  and (ii) the highly connected network structures typical of brain networks (Bullmore and Sporns, 2009); these are known to violate irrepresentable and incoherence conditions that are necessary for perfect graph selection (Meinshausen and Bühlmann, 2006; Ravikumar et al., 2011; Cai, Liu and Luo, 2011).

2.2. *Challenge I: Two Levels of Network Variability.* For our two-level problem (1), we must account for two sources of network variability when conducting population inference: (i) variability between subjects within a group and (ii) variability of the network selection procedure within a single subject. To see this, let us study a real multi-subject fMRI example. In Figure 2, we show estimated functional brain networks for subjects from the UCLA fMRI ABIDE data set (INDI, 2013). We describe the details of this data set, our pre-processing, and brain parcellation later in the Case Study in Section 5. In the top and middle panels, we estimate brain networks for each subject using graph selection methods for Gaussian graphical models (see Section 3.1 for details) and plot these as circle graphs to easily visualize network differences. It is clear that there are not only differences between autistic subjects and control subjects, but there is also large heterogeneity across subjects within each group. This is well-known in the neuroimaging literature (Milham et al., 2012; Nielsen et al., 2013), and makes finding statistically significant differences between subject groups much more challenging.

Less well studied in neuroimaging, is the second source of variability which arises from *estimating* networks for each subject instead of directly observing the networks. In the bottom panel of Figure 2, we re-estimate brain networks for a single control subject with bootstrap resampled data. It is clear that there is major intra-subject variability arising from our graph selection procedure. Indeed in neuroimaging, test-re-test studies which conduct brain imag-

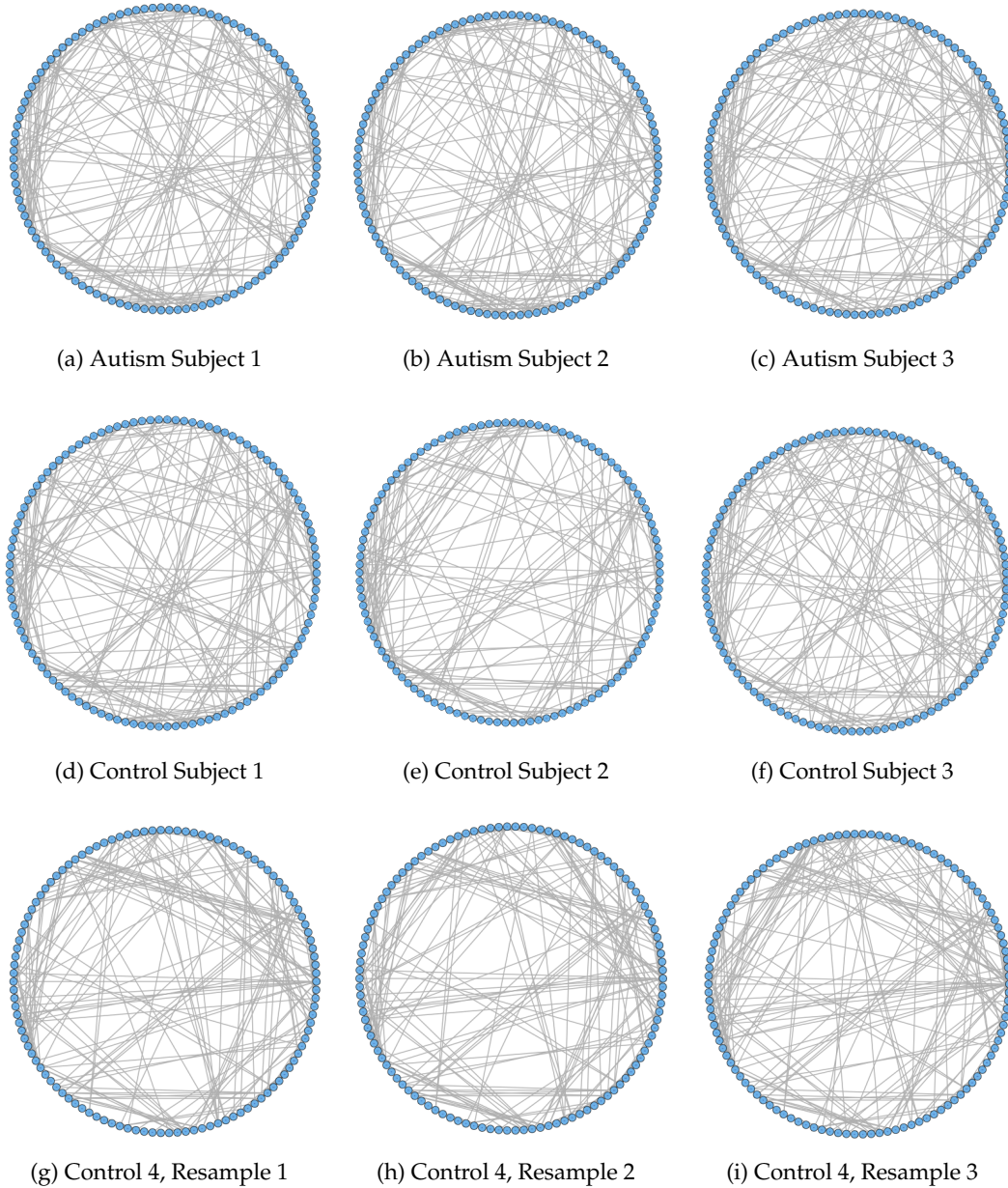


Figure 2: Motivating example of both inter- and intra-subject network variability in estimated functional brain networks. Gaussian graphical models were used to estimate networks from the UCLA ABIDE fMRI data set (INDI, 2013) that we work with further in Section 5 for three autistic subjects (top), three control subjects (middle), and three bootstrap resampled data sets from a control subject (bottom). To conduct population inference across two groups, we must account for both the network variability between subjects (top and middle panels) as well as the variability associated with network estimation within a single subject (bottom panel). This also motivates the applicability of our two-level model, (1), for population network inference.

ing on the same subject in repeated sessions have shown high variability in the subject’s estimated brain networks (Wang et al., 2011). This also motivates the necessity of using a two-level model like (1) for population network inference as opposed to the one-level model and test statistics of the standard procedure.

Now, let us consider the consequences of these two levels of network variability for our specific model and edge testing problem. Studying the variability via the post selection distribution of the estimated networks,  $\hat{\Theta}^{(i)}$ , is a major challenge that has not yet been tackled in the statistics literature. Thus, a direct approach to conducting population inference for the model (1) is beyond the scope of this paper and something that is saved for future work. Instead, we opt to break this problem into a series of simpler ones in an approach that is more closely aligned with the standard procedure: We consider a separate two-level model for each edge in the network that can capture the two sources of network variability.

To model the two sources of network variability for each edge, we turn to the commonly used Beta-Binomial model (Searle, Casella and McCulloch, 2009). As presented earlier, let  $Y_{k,l}^{(i)} = \mathbb{I}(\theta_{k,l}^{(i)} \neq 0)$  denote the edge support statistic for the  $(k, l)^{th}$  edge associated with the  $i^{th}$  subject graphical parameter (precision matrix)  $\Theta^{(i)}$ . Since each estimated network is a random variable,  $Y_{k,l}^{(i)}$  is a random variable whose variability is related to the selection variability of our estimated network for subject  $i$ . Let  $\mu_{(k,l)}^{(i)} = \mathbb{P}(\theta_{(k,l)}^{(i)} \neq 0)$  be a new parameter denoting this subject-level probability of observing an edge at  $(k, l)$  in the  $i^{th}$  subject; we model the selection variability in the  $i^{th}$  subject as  $Y_{k,l}^{(i)} \sim \text{Bern}(\mu_{(k,l)}^{(i)})$ . But, the edge selection probabilities for each subject are themselves random variables related to the group-level probabilities for each edge. A common model for such probabilities is the beta distribution; thus, we let  $\mu_{(k,l)}^{(i)} \sim \text{Beta}(\alpha_{(k,l)}^g, \beta_{(k,l)}^g)$ . Typically, a reparameterization of this model is used where  $\pi_{(k,l)}^g = \alpha_{(k,l)}^g / (\alpha_{(k,l)}^g + \beta_{(k,l)}^g)$  denotes the mean,  $\mathbb{E}(\mu_{(k,l)}^{(i)}) = \pi^g$ , of the Beta distribution, and where  $\rho_{(k,l)}^g = 1 / (\alpha_{(k,l)}^g + \beta_{(k,l)}^g + 1)$  is related to the variance of the Beta distribution given by  $\text{Var}(\mu_{(k,l)}^{(i)}) = \rho_{(k,l)}^g \pi_{(k,l)}^g (1 - \pi_{(k,l)}^g)$  (Searle, Casella and McCulloch, 2009). Suppose we also observe  $m$  iid observations from this model and let  $Z_{(k,l)}^{(i)} = \sum_{j=1}^m Y_{j,(k,l)}^{(i)}$ . Then, we arrive at the familiar form of the Beta-Binomial model:

$$(3) \quad Z_{(k,l)}^{(i)} | \mu_{(k,l)}^{(i)} \stackrel{iid}{\sim} \text{Bin}(\mu_{(k,l)}^{(i)}, m), \quad \mu_{(k,l)}^{(i)} \stackrel{iid}{\sim} \text{Beta}(\pi_{(k,l)}^g, \rho_{(k,l)}^g).$$

This Beta-Binomial model, which is often used to model over-dispersed binary data, is ideal for modeling both the intra-subject selection variability and the inter-subject group-level variabilities of each edge. To see this, consider the unconditional variance of  $Z_{(k,l)}^{(i)}$  which incorporates two levels of variability as follows (for convenience, we suppress the edge indices):

$$(4) \quad \begin{aligned} \text{Var}(Z^{(i)}) &= \sum_j \text{Var}(Y_j^{(i)}) + \sum_{j < j'} \text{Cov}(Y_j^{(i)}, Y_{j'}^{(i)}) \\ &= m\pi^g(1 - \pi^g) + \underbrace{m(m-1)\rho^g\pi^g(1 - \pi^g)}_{\text{Additional Binomial Variation}}. \end{aligned}$$

Hence, the first term represents variability across subjects in group  $g$  and the second term represents the variability associated with the selection procedure within subject  $i$ , a quantity

that we assume to be constant across subjects  $i$  in each group  $g$ . Consider now what happens if our true model follows this two-level Beta-Binomial model, but as with the standard approach, we use a one-level Binomial model and associated two-sample test statistic. The variance is thus underestimated and the test statistic is overoptimistic. Then, when inference is conducted for the population mean  $\pi^g$ , using the incorrect Binomial model leads to inflated Type I error rates; this behavior has been well-documented (Weil, 1970; Liang and Hanfelt, 1994). Hence, failure to use the correct two-level model which accounts for the two levels of network variability partially explains the high error rates of the standard procedure observed in Figure 1.

Notice in (3) that we have defined our Beta-Binomial model for the edge selection probabilities assuming that we have multiple iid observations from this model. For real fMRI data, we typically only have one scanning session per subject and hence only one estimate of the functional connectivity network,  $\Theta^{(i)}$ , per subject. Then with only one observation,  $Y_{(k,l)}^{(i)}$ , for each subject, the Beta-Binomial model for each edge reduces to a Beta-Bernoulli model. In this model, the correlation parameter,  $\rho^g$ , is unidentifiable and the intra-subject variability associated with graph selection cannot be estimated. Thus, estimating the two-levels of network variability from data with only one observation is a challenge; in Section 3.2, we discuss how we address this by using resampling techniques to estimate the second source of network variability.

*2.3. Challenge II: Graph Selection Errors.* In the previous section, we deconstructed our problem into a two-level model for each edge to simplify modeling the two sources of variability. The models for each edge, however, are clearly not independent as we are modeling the network support for a population of Gaussian graphical models. Here, we discuss how dependencies in the population network structure can lead to graph selection errors that bias the estimates of our group-level edge parameters. These in turn lead to false positives and false negatives when conducting inference at the group level.

Note that as previously discussed, we are working under the regime where we cannot obtain perfect estimates of the network support, as this is the most realistic scenario for real fMRI data. Thus, it is constructive to understand the conditions under which perfect network recovery or graph selection consistency is achievable so that we can understand the consequences when these conditions are violated. Meinshausen and Bühlmann (2006) first introduced an irrepresentable condition for neighborhood selection-based estimation of GGMs that closely follows from irrepresentable or incoherence conditions for the lasso regression problem Zhao and Yu (2006). Later, Ravikumar et al. (2011) characterized a log-determinant based irrepresentable condition corresponding to estimating GGMs via penalized maximum likelihood, or the so-called graphical lasso method (Rothman et al., 2008; Friedman, Hastie and Tibshirani, 2008). This condition places restrictions on the Fisher information matrix,  $\Gamma = \Theta^{-1} \otimes \Theta^{-1}$ ; that is, if we let  $S$  denote the network support and let  $S^C$  denote the non-support, then the condition requires that  $\|\Gamma_{S^C,S}^T (\Gamma_{S,S})^{-1}\|_\infty \leq 1 - \eta$ , for some  $0 < \eta < 1$ . In addition to irrepresentability conditions, the eigenvalues of the restricted Fisher information  $(\Gamma_{S,S})^{-1}$  as well as covariance matrix  $(\Theta^{-1})_S$  need to be bounded away from zero, and the entries of the precision matrix  $\Theta_{(k,l)}^i$  need to satisfy signal strength conditions in order to prevent false exclusions of edges in each subject (Ravikumar et al., 2011). Both neighborhood and log-determinant irrepresentable conditions limit the amount of correlation within true edges and between true edges and non-edges; this, then places

severe restrictions on the model space and types of network structures where graph selection consistency is achievable. As illustrated in [Meinshausen \(2008\)](#), certain simple network structures nearly guarantee irrepresentable conditions are violated in the population version, and consequently in finite samples. For example, estimators have a high probability of incorrectly selecting an edge connecting two nodes that share similar node-neighborhoods. Now, let us return to our problem of conducting group level inference in situations where we know that the irrepresentable-type conditions are violated. Differentially present edges in one group of subjects can change the network structure in a manner that graph selection errors are more likely to occur in one group. Thus, these group-level estimates will be biased. Following our procedure, biased group-level edge probability estimates will then bias test statistics and lead to a higher probability of false positives or false negatives for group-level inference.

To better understand this, we offer a small illustration in [Figure 3](#). For simplicity, we assume that the group-level probabilities for each edge in [\(1\)](#) are  $\{0, 1\}$ , meaning that we assume all subjects within a group share the same network structure. First in the left panel of [Figure 3 \(a\)](#), we assume that all subjects in the population share the common edges in black, but that subjects in group two have a differentially present edge connecting (1,2). Since nodes 1 and 2 share common node-neighborhoods, an edge between (1,2) is selected with high probability in both group 1 and group 2 subjects. The group 1 estimate of edge probability (1,2) will then be biased and lead to a false negative when conducting inference across the groups. Similarly in the left panel of [Figure 3 \(b\)](#), all subjects in group two have an additional differential edge connecting (2,5). Unlike in group 1, when (2,5) are connected in group 2, nodes 4 and 5 are also highly correlated due to common node neighborhoods. Thus graph selection in group 2 will estimate an edge at (4,5) with high-probability, whereas graph selection will be more likely to estimate the correct network in group 1. This results in a biased estimate for edge (4,5) in group two, leading to a false positive at (4,5) when conducting inference at the group level. Thus even for simple graph structures, the location of differentially present edges in the network structure can lead to graph selection errors that bias group-level estimates and lead to false positives and false negatives for group-level inference. With more complicated network structures, this problem will be further exacerbated.

In general, group-level biases in the edge probability estimates will occur when graph selection consistency does not hold for each subject. It is then difficult to control the overall error rates of any inferential procedure at the group level. Analogous to standard irrepresentability conditions, we conjecture that there exists irrepresentability-like conditions for our problem [\(2\)](#), that limit the correlation between differential and non-differential edges of the graph. That is, differentially present edges cannot be too correlated with common edges (as illustrated in [Figure 3 \(a\)](#)) and differentially present edges cannot be too correlated with non-edges (as illustrated in [Figure 3 \(b\)](#)). While proving such conditions is beyond the scope of this paper, we explore these empirically in [Section 4](#). Note that as we expect large violations of irrepresentable-like conditions with real fMRI data, it may be unrealistic to expect that this problem can be fully solved and error rates properly controlled. However, we would expect that any method that weakens irrepresentability conditions for graph estimation at the subject level will ameliorate biases in group-level edge estimates and lead to an inferential procedure with both higher statistical power and a lower false positive rate.

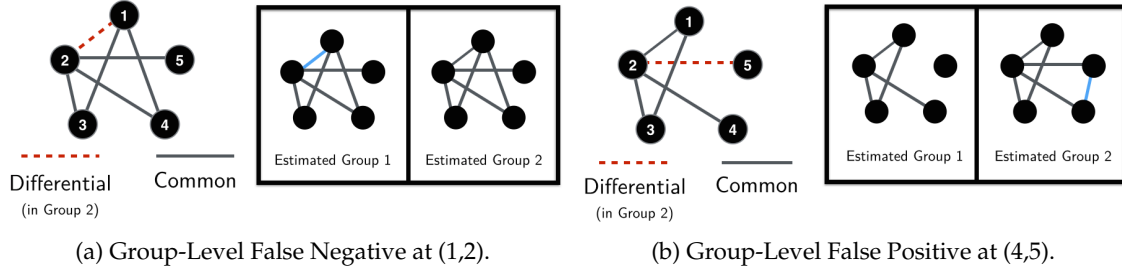


Figure 3: Illustration of group level biases stemming from graph selection errors that would result in false negatives (a) and false positives (b) for group inference. In each figure, true graphs for a simple 5-node network are given on the left and estimated graphs on the right. In (a), an edge is likely to be selected at (1,2) in group one, resulting in a bias that would yield a false negative at the group-level. In (b), an edge is likely to be selected at (4,5) in group two, resulting in a bias that would yield a false positive at the group-level.

**3. The  $R^3$  Method.** We develop a novel procedure to conduct two-sample inference for our problem (2), namely, testing for the differential presence / absence of edges across a population of networks. Our approach integrates the network estimation and inference problems to address the two popPSI challenges outlined in Section 2. To achieve this, we employ three key ingredients - resampling, random penalization, and random effects; hence we call our procedure  $R^3$ .

In this section, we briefly discuss each of the components of the  $R^3$  procedure separately before putting them all together in Section 3.5. As discussed in Section 2.2, we use two level models at the edge level to account for estimation variability as well as between subject variability of networks. However, we only observe one network per subject. In the absence of multiple networks per subject, we use bootstrap resampling to generate network replicates for each subject, Section 3.2. We then use a beta-binomial model to model the two-level edge probabilities and employ a beta-binomial two-sample random effects test statistic to aggregate our edge statistics over the two levels, Section 3.4. Thus, the resampling plus random effects portion of our procedure solves the first popPSI challenge. The second popPSI challenge of graph selection errors that bias edge probability estimates is more difficult to directly solve. We can dramatically ameliorate the affect of these errors, however, by using a technique introduced by [Meinshausen and Buhlmann \(2010\)](#) - random regularization penalties, discussed in Section 3.3. Random penalties in conjunction with our resampling procedure thus address the second popPSI challenge. As subject-level network estimation is integral to the entire  $R^3$  procedure, we begin by discussing how we estimate each functional brain network.

**3.1. Preliminaries: Subject Graph Estimation.** Our proposed  $R^3$  framework is compatible with any graph selection procedure for Gaussian graphical models. A popular method for estimating inverse covariances is the so-called *graphical lasso* or penalized maximum likelihood method, ([d’Aspremont, Banerjee and El Ghaoui, 2006](#); [Friedman, Hastie and Tibshi-](#)

rani, 2008), which solves the following objective:

$$(5) \quad \hat{\Theta}_{\lambda_i}^i(X^{(i)}) = \arg \min_{\Theta > 0} \mathcal{L}(\hat{\Sigma}^i; \Theta) + \lambda_i \|\Theta\|_{1,\text{off}} = \arg \min_{\Theta > 0} \text{Tr}(\hat{\Sigma}^i \Theta) - \log \det(\Theta) + \lambda_i \|\Theta\|_{1,\text{off}}$$

where  $\hat{\Sigma}^i$  is the empirical sample covariance,  $\hat{\Sigma}^i = \frac{1}{T}(X^{(i)\text{T}}X^{(i)})$  and  $\|\Theta\|_{1,\text{off}} = \sum_{k < l} |\theta_{k,l}|$  is the  $\ell_1$  penalty on off-diagonals. Other estimation procedures such as the neighborhood selection of Meinshausen and Bühlmann (2006) or the CLIME estimator of Cai, Liu and Luo (2011) could also be employed. In this paper, we obtain  $\hat{\Theta}$  using the QuIC implementation by Hsieh, Sustik and Ravikumar (2011). From hereon, we denote the presence of the  $(k, l)$  edge, selected by any graph estimation procedure as:

$$(6) \quad Y_{(k,l)}^i | \hat{\Theta}_{\lambda_i, (k,l)}^{(i)}(X^{(i)}) = \mathbb{I}(\hat{\Theta}_{\lambda_i, (k,l)}^{(i)}(X^{(i)}) \neq 0)$$

While inverse covariance estimation assumes that  $X^i$  consists of independent observations from the multivariate normal, resting-state fMRI data consists of dependent observations. Thus, neuroimaging data effectively consists of fewer than  $T$  independent observations and is often well-described by an autoregressive process (Worsley et al., 2002). Hence, we first use an autoregressive model to whiten the time series and the Ljung-Box test to verify that whitened observations are independent before applying graph selection procedures.

Notice, that we also need to estimate the regularization parameter,  $\lambda_i$ , controlling the graph sparsity for each subject. In the standard approach, sparsity levels are typically fixed across all subject networks (Bullmore and Sporns, 2009). As our procedure tests for differential sparsity, however, we cannot enforce identical graph sparsity for each subject. Hence, we need a good initial estimate of  $\lambda_i$ . While there are several model selection procedures proposed for graph selection, we employ the StARS procedure of (Liu, Roeder and Wasserman, 2010).

3.2.  $R^3$ : Resampling. Recall that, as discussed in Section 2.2, one of the challenges with popPSI is accounting for two-levels of network variability when we typically obtain only one network estimate per subject. We address this by using resampling, specifically bootstrapping (Efron and Tibshirani, 1993), to obtain both a better estimate of the network and its variability. We also note that as we discuss in the next section, resampling will also be critical in addressing the second popPSI challenge.

For each subject  $i$ , we sample  $T$  out of  $T$  observations with replacement yielding the bootstrapped data,  $X^{*b,(i)}$ . We then apply a graph selection procedure to this bootstrapped data which gives us the bootstrapped edge selection statistic  $Y_{(k,l)}^{*b,i} | \hat{\Theta}_{\lambda_i, (k,l)}^{*b,(i)}(X^{*b,(i)})$ . While we could estimate the edge-level probability for each subject by  $\tilde{\mu}_{(k,l)}^{(i)} = Y_{(k,l)}^i$ , we could also use bootstrap aggregation (Breiman, 1996) yielding  $\hat{\mu}_{(k,l)}^{(i)} = \frac{1}{B} \sum_{b=1}^B Y_{(k,l)}^{*b,i}$ . Many have recently shown the benefits of using resampling for graph selection with error control (Bach, 2008; Meinshausen and Bühlmann, 2010; Li et al., 2011; Liu, Roeder and Wasserman, 2010). Thus, we prefer the resampled statistic  $\hat{\mu}^i$  to  $\tilde{\mu}^{(i)}$ . Although we cannot expect our estimate to be unbiased for  $\mu_{(k,l)}^i$  in high-dimensional settings or for highly connected network structures (as discussed in Section 2.3), Meinshausen and Bühlmann (2010) and Shah and Samworth (2013) have shown that stability based statistics more effectively separate true and false edges. For

our  $R^3$  procedure, we will use resampling to not only improve estimation of edge selection probabilities, but also to estimate variability for two-level random effects models and with random penalization procedures as discussed subsequently.

3.3.  $R^3$ : *Random Penalization*. As discussed in Section 2.3, graph selection errors can bias estimates of edge selection probabilities which in turn lead to errors when conducting inference at the group level. For real fMRI data with limited samples  $T$  and highly connected network structures that violate irrepresentable-type conditions, we will likely never be able to fully solve the problems induced by graph selection errors. Here, we try to ameliorate their affect by employing random penalization techniques recently introduced by [Meinshausen and Buhlmann \(2010\)](#). For each bootstrap sample  $b = 1, \dots, B$ , we generate a  $p \times p$  symmetric matrix of regularization parameters that randomly penalizes each edge, denoted  $\Lambda^{bi}$ . We employ random penalization that modifies the objective, (5), through an element-wise weighted penalty:

$$(7) \quad \hat{\Theta}_{\Lambda^{bi}}^i = \arg \min_{\Theta > 0} \left( -2\mathcal{L}(\hat{\Sigma}^{bi}, \Theta) + \|\Lambda^{bi} \circ \Theta\|_1 \right)$$

where  $\circ$  is the element-wise Hadamard product. Our matrix of random penalties,  $\Lambda^{bi}$ , is obtained by perturbing the initial pilot estimate of the regularization parameter for each subject,  $\lambda^i$ , as follows:

$$(8) \quad \Lambda_{kl}^{bi} = \lambda^i + c \lambda_{max}^i W_{k,l} \quad \forall k < l$$

where  $\Pr\{W_{k,l} = \pm 1\} = \frac{1}{2}$ ,  $c \in (0, .5)$  is fixed as a small fraction, and  $\lambda_{max}^i$  is the regularization parameter for each subject that results in the fully sparse graph. Thus, our random perturbation procedure can be seen to penalize each edge independently as  $\lambda \pm c\lambda_{max}$ ; for our purposes, we have found that  $c = .25$  performs well. Note that our random penalties are different than the conservative scheme proposed by [Meinshausen and Buhlmann \(2010\)](#) for the purpose of controlling false positive edge selection. Other alternatives such as using  $c \sim U(0, .5)$  are also possible, and are closely related to the procedure of [Li et al. \(2011\)](#) who aggregate edge selection frequencies over a range of perturbations of  $\lambda$ .

Intuitively, our randomized regularization scheme decreases the influence of the inclusion or exclusion of any given edge on the selection of other edges. Thus, we expect our approach to improve the problems associated with graph selection discussed in Section 3.1. In fact, several have recently shown that restricted eigenvalue and irrepresentability-type conditions can be violated for the original data, but hold when aggregating selection over random penalizations ([Meinshausen and Buhlmann, 2010](#); [Bühlmann, van de Geer and Van de Geer, 2011](#)). Hence, with random penalization, consistent graph selection can be achieved while tolerating larger correlations between variables. For our popPSI problem, we expect that random penalization will allow us to tolerate more correlation between differential edges and common edges, and differential edges with non-edges. We empirically study this intuition through simulations in Section 4.

3.4.  $R^3$ : *Random Effects*. Recall that in Section 2.2 we introduced a Beta-Binomial model, (3), to account for the two sources of network variability at the edge level. With only one estimated network, however, estimating two levels of variability and fitting the Beta-Binomial model was not possible. Now, we can use our bootstrap resampled data to properly fit the

Beta-Binomial model and obtain the corresponding two-sample test statistics for each edge. For each subject  $i$  and each edge  $(k, l)$ , we obtain  $B$  resampled edge statistics,  $Y_{(k,l)}^{b,i}$ . Suppressing the edge indices for notational simplicity, we then have that  $Z^{*,i} = \frac{1}{B} \sum_{b=1}^B Y^{b,i}$  is our statistic associated with the subject edge probability,  $\mu_i$ . Hence, we can re-write the Beta-Binomial model given in (3) for our bootstrapped statistics:

$$(9) \quad Z^{*,i} | \mu^{(i)} \stackrel{iid}{\sim} \text{Bin}(\mu^{(i)}, B), \quad \mu^{(i)} \stackrel{iid}{\sim} \text{Beta}(\pi^{(g)}, \rho^{(g)}).$$

Recall that the Beta-Binomial model is often used for over-dispersed or group-correlated binary data (Crowder, 1978). Our bootstrapped edge statistics over the subjects certainly fit this model as bootstrapping results in positively correlated statistics within each subject (Bickel, Götze and van Zwet, 2012). As previously noted, this model also nicely captures the variability of edge support both within and between subjects.

We propose to fit our Beta-Binomial model via the widely used moment estimators for  $\pi$  and  $\rho$  (Kleinman, 1973). For estimation, assume that we will always have a balanced number of bootstrap samples per subject. Then estimates for  $\pi$  and  $\rho$  as proposed by Kleinman (1973); Ridout, Demétrio and Firth (1999) are as follows:

$$(10) \quad \hat{\pi}_g = \frac{1}{n_g} \sum_{i \in \mathcal{G}_g} Z^{*,i} \quad \& \quad \hat{\rho}^g = \frac{B}{B-1} \frac{\sum_{i \in \mathcal{G}_g} (\hat{\pi}^g - Z^{*,i})^2}{\hat{\pi}^g (1 - \hat{\pi}^g) (n_1 - 1)} - \frac{1}{B-1}.$$

These estimators are consistent for  $\pi$  and  $\rho$  (Moore, 1986) and are asymptotically normal (Kleinman, 1973). For balanced data such as in our case, these estimators exhibit only mild loss of efficiency compared to more commonly used likelihood-based estimators (Kleinman, 1973). We choose to employ these estimators, however, as they are very simple to compute and widely used when conducting inference on  $\pi$  as in our problem. Specifically for inference on  $\pi$ , it is well-known in the teratological literature that failure to account for  $\rho$  results in inflated Type I error rates (Weil, 1970; Liang and Hanfelt, 1994), but this inference has also been shown to be robust to various estimators for  $\rho$  (Moore, 1986). Further, many have shown that for balanced data as in our case, the moment estimators for  $\pi$  and  $\rho$  give empirical Type I error control when conducting inference on  $\pi$  (Ridout, Demétrio and Firth, 1999; Liang and Hanfelt, 1994; Liang and Self, 1996). Given this wide literature, we thus opt to use the computationally simpler moment estimators (10) to fit our Beta-Binomial model.

With these estimators, we develop a two-sample Wald test statistic appropriate for our hypothesis (2). To this end, we need an estimate of the sampling variance of  $\hat{\pi}^g$ . Following from (4) and using our estimates of  $\hat{\pi}^g$  and  $\hat{\rho}^g$ , we can easily see that an estimate of the variance of  $\hat{\pi}^g$  is given by:

$$s_g^2 = \frac{\hat{\pi}^g (1 - \hat{\pi}^g)}{m(n_g - 1)} (1 + (m - 1)\hat{\rho}^g).$$

Putting everything together, we then arrive at the following two-sample Wald test-statistic for our problem (2):

$$(11) \quad \mathcal{T} = \frac{\hat{\pi}^A - \hat{\pi}^B}{\text{se}(\hat{\pi}^B - \hat{\pi}^B)} = \frac{\hat{\pi}^A - \hat{\pi}^B}{\sqrt{\frac{s_A^2 (n_A - 1)}{n_A} + \frac{s_B^2 (n_B - 1)}{n_B}}}.$$

Following from [Kleinman \(1973\)](#), this test statistic is asymptotically standard normal as  $n_A$  and  $n_B \rightarrow \infty$ . In fMRI studies, however, our sample sizes are typically small. Thus, we favor comparing our test statistic  $\mathcal{T}$  to a permutation null distribution to obtain  $p$ -values ([Janssen, 1997](#); [Nichols and Holmes, 2002](#)).

---

**Algorithm 1**  $R^3$  := Resampling, Random Penalization and Random Effects Procedure

---

1. For each subject,  $i = 1, \dots, n$ , obtain pilot estimates of the regularization parameter  $\lambda_i$ . (Section 3.1)
  2. RESAMPLING AND RANDOM PENALIZATION:  
For  $b = 1, \dots, B$ :
    - (a) Bootstrap data yielding  $\mathbf{X}^{*i,b}$ .
    - (b) Fit weighted graphical lasso using random penalty matrix in Eq. (8) giving  $\hat{\Theta}(\mathbf{X}^{*i,b})$ . (Section 3.3)
    - (c) Record edge support statistics  $Y_{k,l}^{*i,b} = I(\hat{\theta}_{(k,l)}^{*i,b} \neq 0)$ .
 End.
  3. EDGE FILTERING: Eliminate edges absent from both groups from consideration, giving the set  $\mathcal{E}_F$  for testing. (Section 3.5)
  4. INFERENCE:
    - For  $(k, l) \in \mathcal{E}_F$ :
      - i. Compute test statistics  $\mathcal{T}_{(k,l)}$  as in Eq. (11) (Section 3.4)
      - ii. Calculate  $p$ -values using a permutation null distribution for  $\mathcal{T}_{(k,l)}$ .
 End.
    - iii Correct for multiplicity via the Benjamini-Yekutieli procedure.
- 

3.5. *The  $R^3$  Procedure.* Now, we are ready to put our whole  $R^3$  procedure together. We outline our procedure in Algorithm 1 for conducting inference on the differential presence of all edges in a population of graphical models, (2). Note that testing all edges would result in an ultra-large-scale inference problem as there would be  $\binom{p}{2}$  hypotheses tested. This is clearly ill-advised; especially so since for brain connectivity networks, we expect rather sparse networks meaning that most edges are absent from both population groups. Thus, we limit our consideration to only the edges that are present in at least one of the population groups:

$$\mathcal{E}_F^c \triangleq \{(k, l) : Z_{(k,l)}^{*i} \leq B\tau, \forall i = 1, \dots, n\}$$

We filter out all edges that have edge proportions less than  $\tau$  for all subjects, leaving our filtered edge set,  $\mathcal{E}_F$ . Notice that filtering is agnostic to group membership and thus does not affect group-level inference. We suggest taking  $\tau \in (.2, .5)$  which typically reduces the number of edges under consideration from thousands to hundreds for real fMRI data. Additionally, we must correct for multiple testing. As our test statistics will be highly dependent, we suggest using the Benjamini-Yekutieli procedure ([Benjamini and Yekutieli, 2001](#)) which controls the false discovery rate under arbitrary dependencies. Finally, we note that instead of testing all edges, our procedure could also be used to test targeted hypotheses regarding specific edges.

**4. Simulation Studies.** We study our  $R^3$  procedure through a series of simulations, showing that  $R^3$  substantially improves statistical power and error control for our popPSI problem, (2). We will particularly study how our method and the standard approach address each of the challenges outlined in Section 2.

4.1. *Simulation Setup.* Henceforth, we will denote the components of  $R^3$  as Resampling (RS), Random Penalization (RP) and Random Effects (RE). To better understand how each challenge outlined in Section 2 as well as the our methodological solutions to these challenges affect inferential procedures, we compare  $R^3$  not only to the standard approach but also variations of our own method:  $R^2$  with (RS, RP) and  $R^2$  with (RS, RE). Recall from Section 2, that the standard approach uses two-sample test statistics associated with the one-level Binomial distribution. Both the numerator and denominator of this test statistic are incorrect, with the mean group level parameters biased by graph selection errors (Challenge II in Section 2.3) and with the denominator under-estimating the variance components associated with two levels of network variability (Challenge I in Section 2.2). Our first variant,  $R^2 = (\text{RS}, \text{RP})$ , seeks to address only Challenge II by ameliorating the bias in group-level edge proportions using random penalization. Our second variant,  $R^2 = (\text{RS}, \text{RE})$  seeks to address only Challenge I by using the correct two-level Beta-Binomial model and test statistics. We adopt the same specifications outlined in Section 3.5 with  $\lambda_i$  selected using StARS (Liu, Roeder and Wasserman, 2010) for all methods. Methods including the RE component use random effect statistics from Section 3.4, while those without RE use the standard two-sample binomial proportions test as in Section 2.2. We control FDR at 10% for all methods using the Benjamini-Yekutieli approach (Benjamini and Yekutieli, 2001).

We study several simulation scenarios to fully test our methods. First, we generate multivariate observations,  $X_{T \times p}^{(i)}$ , for each subject according to  $\mathcal{N}(0, (\Theta^{(i)})^{-1})$ . We simulate the strength of connections for all edges as  $\theta_{(k,l)}^i \sim \text{Uniform}([-1.25, -1] \cup [1, 1.25])$ , and then add a sufficient amount to the eigenvalues of  $\Theta^i$  to ensure positive definiteness. Each group consists of a balanced number of subjects,  $n_1 = 20$  and  $n_2 = 20$ , and we consider a moderate dimensional case with  $p = 50, T = 400$ ; we set approximately 150 edges to be differentially present and evenly divide these between the two groups. Second, as functional connectivity is known to exhibit small world and hub-like network structures (Achard et al., 2006), our simulated network models follow a challenging banded, small world, or hub-like structure. Third, as the location of common and differential edges in the population network structure can lead to bias in the group-level edge estimates (discussed in Section 2.3), we set the location of differential edges to follow two schemes, referred to as Case I and Case II. In Case I, we consider *Clustered Differential Edges* in which differential edges in one group are highly correlated with other differential edges as well as common edges. In Case II, we consider *Random Differential Edges* where the differential edges occur at random throughout the network structure. Thus, we expect Case I to violate our conjectured irrepresentable-type conditions under which unbiased estimation of the edge probability and hence overall error control of the inferential procedures is achievable; Case II should ameliorate these conditions. Combining graph types for each of these cases results in a total of six simulations. To simplify our investigation into these six simulation scenarios (results shown in Figure 4 and Table 1), we set  $\pi_{(k,l)}^s = 1$  for all edges.

We investigate changing  $\pi^s$  for differentially present edges by setting  $\pi_{(k,l)}^s = \{1, .5, .3\}$  in a separate simulation (Figure 5) for the banded and hub-type graphs for Case II type differ-

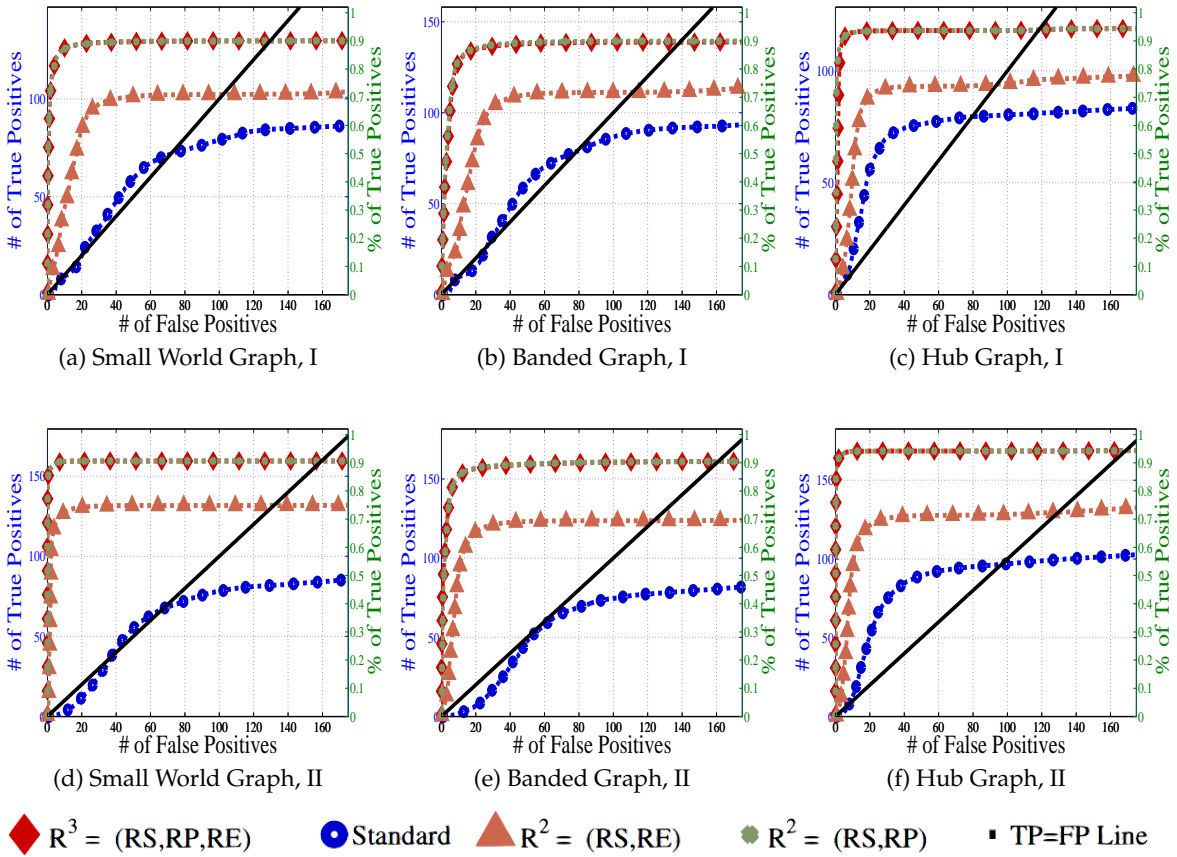


Figure 4: Average ROC curves for sequentially rejected tests comparing our method to the standard approach,  $R^2 = (RS, RE)$ , and  $R^2 = (RS, RP)$  for each network structure type and Case I and II type differential edges. Methods employing random penalization (RP) improve statistical power as they ameliorate graph selection errors that bias group-level estimates.

ential edges. For this simulation, we use population correlations rather than covariances in order to eliminate variations in scale across subjects. Additionally for fair comparisons here, we limit the number of differential edges to 25 per group and fix the degree of the common support to be  $0.12p$ .

Further simulations studies as well as additional supporting material for our simulations can be found in the supplementary materials (Narayan, Allen and Tomson, 2015a). These include confusion adjacency matrices showing the location of false positives and false negatives in the network structure for all methods, an analogous simulation study in a high-dimensional setting  $p > T$ , and a study of the impact of graph sparsity for both common and differential edges on our methods.

4.2. *Results.* In Figure 4 and Table 1, we present our main simulation results comparing  $R^3$  to the two variations of our  $R^2$  method and the standard approach for three network structures and Case I and II type differential edges. First for Figure 4, we report results in terms of operating characteristics averaged across 50 replicates with the number of true

Case	Sim Type	Metric	$R^3$		Standard Test		$R^2 = (RS, RE)$		$R^2 = (RS, RP)$	
I	SmallW	TPR	0.934	(0.036)	0.542	(0.096)	0.739	(0.082)	0.937	(0.037)
		FDP	0.245	(0.079)	0.661	(0.028)	0.476	(0.040)	0.643	(0.016)
I	Banded	TPR	0.921	(0.069)	0.524	(0.105)	0.735	(0.091)	0.933	(0.038)
		FDP	0.261	(0.122)	0.645	(0.039)	0.446	(0.053)	0.624	(0.041)
I	Hub	TPR	0.967	(0.021)	0.616	(0.131)	0.763	(0.099)	0.968	(0.021)
		FDP	0.107	(0.056)	0.497	(0.040)	0.306	(0.048)	0.474	(0.019)
Case	Sim Type	Metric	$R^3$		Standard Test		$R^2 = (RS, RE)$		$R^2 = (RS, RP)$	
II	SmallW	TPR	0.959	(0.026)	0.483	(0.097)	0.792	(0.071)	0.959	(0.026)
		FDP	0.112	(0.079)	0.659	(0.042)	0.370	(0.037)	0.615	(0.012)
II	Banded	TPR	0.941	(0.044)	0.450	(0.105)	0.724	(0.105)	0.946	(0.043)
		FDP	0.199	(0.095)	0.667	(0.042)	0.425	(0.058)	0.623	(0.018)
II	Hub	TPR	0.971	(0.023)	0.533	(0.133)	0.735	(0.106)	0.972	(0.023)
		FDP	0.051	(0.029)	0.463	(0.046)	0.262	(0.042)	0.406	(0.009)

TABLE 1

Average true positive rate (TPR) and false discovery proportion (FDP) for tests rejected by each method when controlling the FDR at 10% via the Benjamini-Yekutieli method; standard errors are given in parentheses. Methods employing random effects models and test statistics yield improved Type I error rates.

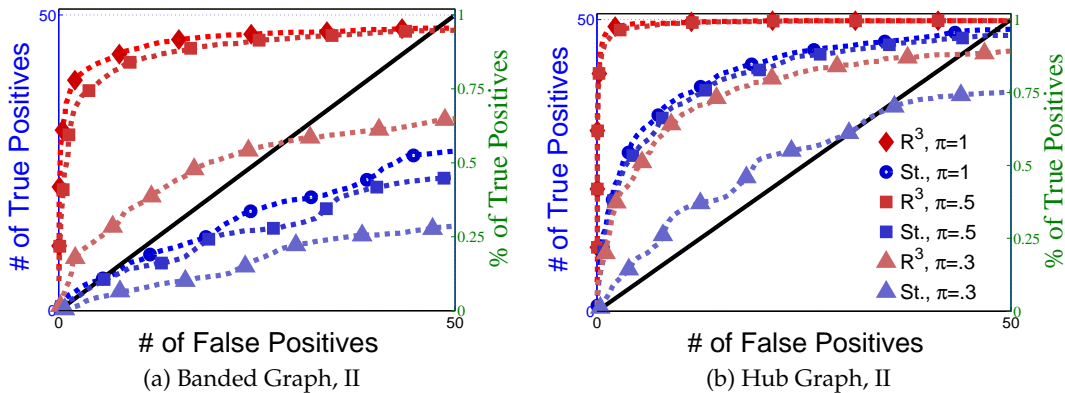


Figure 5: Impact of network variability between subjects. While decreasing  $\pi^s$  for the differentially present edges, we report average ROC curves for sequentially rejected tests for our  $R^3$  method compared to the standard approach for banded and hub-type graphs in Case II scenarios. As the proportion of subjects with differential edges decreases, performance degrades but  $R^3$  continues to well outperform the standard approach.

positives (y-axis) plotted against the number of false positives (x-axis) for each test statistic, rejected sequentially from largest to smallest in absolute magnitude. Overall, all of our methods and particularly  $R^3$  yield substantial improvements over the standard approach in all scenarios.

Notice that both  $R^3$  and  $R^2=(RS,RP)$  share similar orderings of test statistics, and consequently similar ROC curves. Overall, methods that include random penalization yield major improvements in statistical power over those that do not. This indicates that the second popPSI challenge outlined in Section 2.3 is a significant contributor to the poor performance of the standard method. Recall our discussion of how graph selection errors at the subject stage occur non-randomly and hence bias our group-level estimates of  $\hat{\pi}^s$ . Our results empirically demonstrate that random penalization dramatically improves these biases, leading to

less bias in our test statistics and hence improvements in both Type I and Type II error rates. Furthermore, in Case II scenarios where selection errors are moderate, the performance gap between any method containing  $RP$  over  $R^2 = (RS, RE)$  reduces compared to Case I scenarios where selection errors are more severe. Thus, the benefits of random penalization are greater when selection errors are more abundant. Confusion adjacency matrices illustrating the location of inferential errors for our methods shown in the supplemental materials also indicate that random penalization improves graph selection in cases where there are larger correlations between differential edges and common edges. Similar results hold for our high-dimensional study presented in the supplemental material.

Table 1, which accompanies Figure 4, gives the empirical true positive and false discovery rates (FDR) averaged over 50 simulation replicates when the Benjamini-Yekutieli (Benjamini and Yekutieli, 2001) procedure controlling the FDR at 10% is used to determine the number of tests to reject. First, notice that the observed false discovery proportion (FDP) of our  $R^3$  procedure is not 10% on average, indicating that our method does not fully control the FDR. This occurs because we specifically simulate difficult and realistic fMRI scenarios with graph structures that severely violate irrepresentable-type conditions. In situations (not shown) where irrepresentable-type conditions are met that ensure graph selection consistency, our procedure as well as the standard method correctly control the FDR. As discussed in Section 2.3, in situations where graph selection errors occur with high probability, it is likely impossible to provably control the FDR, consistent with our empirical results. Yet even though  $R^3$  does not fully control the FDR, our error rates are dramatically improved over the standard approach and other variations of our procedure.

Also in Table 1, observe that  $R^2 = (RS, RP)$ , which had similarly ordered test statistics to  $R^3$ , has dramatically worse Type I error rates that do not come close to controlling the FDR. While  $R^2 = (RS, RE)$  also does not control the FDR, the error rates are much improved over  $R^2 = (RS, RP)$ . These results demonstrate that using two-level models with the correct random effects test statistics are crucial to Type I error control. Recall from Section 2.2, that using the one-level Binomial model leads to an under-estimation of the variance term which in turn inflates test statistics and leads to an increase in false positives. Note also that the estimated FDP of  $R^3$  is still a major improvement over that of  $R^2 = (RS, RE)$ . This occurs as the problem of graph selection errors induces both Type I and Type II errors. Hence, these results demonstrate the necessity of all three of our  $R^3$  ingredients. Finally, observe that our error rates in Case II scenarios are better than those for Case I scenarios, again indicating that differential edges that are highly correlated with non-edges and common edges pose particular challenges for our popPSI problem. These results are also corroborated in our high-dimensional study presented in the supplemental materials.

Lastly, in Figure 5, we study the effect of letting the network structure vary across subjects by decreasing the differential group edge probability,  $\pi^g$ . Our method continues to perform well for  $\pi^g \in [.5, 1]$ . However, when the differential edge probability drops further to  $\pi^g = .3$ , we see that both  $R^3$  and the standard approach have greatly reduced statistical power, as one would expect. Despite this,  $R^3$  continues to outperform the standard approach.

Overall, our results demonstrate the difficulty of solving the challenges associated with our popPSI problem. In particular, using the correct two-level models are critical to Type I error control while solving or ameliorating the problem of graph selection errors at the subject level are critical for both Type I and Type II error control. Our results also demonstrate the substantial outperformance of our new  $R^3$  method over existing state-of-the-art methods in neuroimaging.

**5. Case Study: Differential Functional Connections in Autism.** We apply our  $R^3$  method to identify differential functional connections associated with Autism Spectrum Disorders (ASD) in a publicly available fMRI study from the Autism Brain Imaging Data Exchange (ABIDE) (INDI, 2013) consortium.

5.1. *fMRI data acquisition and preprocessing.* We use resting state fMRI data from the UCLA Sample 1, (Rudie et al., 2012a; INDI, 2013) which consists of 73 subjects, with 32 controls and 41 subjects diagnosed with Autism Spectrum Disorder (ASD) based on the ADOS or ADI-R criteria. In addition to no history of illness, the controls did not have a first degree relative with autism. The fMRI scans from the UCLA site were acquired when the subjects were passively at rest for 6 minutes using a Siemens 3 T Trio. (T2\*-weighted functional images: TR = 3000 ms, TE = 28 ms, matrix size  $64 \times 64$ , 19.2 cm FoV, and 34 4-mm thick slices (no gap), interleaved acquisition, with an in-plane voxel dimension of  $3.0 \times 3.0$  mm). This results in a total of 120 images per subject. We preprocess the data minimally using FMRIB’s Software Library ([www.fmrib.ox.ac.uk/fsl](http://www.fmrib.ox.ac.uk/fsl)). These steps include brain extraction, spatial smoothing of the images using a Gaussian kernel with FWHM = 5mm, band-pass filtering ( $.01\text{Hz} < f < 0.1\text{Hz}$ ) to eliminate respiratory and cardiovascular signals, and registering images to standard MNI space. We parcellate the images using the anatomical Harvard-Oxford Atlas (Desikan et al., 2006) to obtain 113 regions of interest. We average all voxel time-series within a region to obtain a single time-series per region. Thus, our final processed data matrix consists of 113 regions  $\times$  120 time points  $\times$  73 subjects.

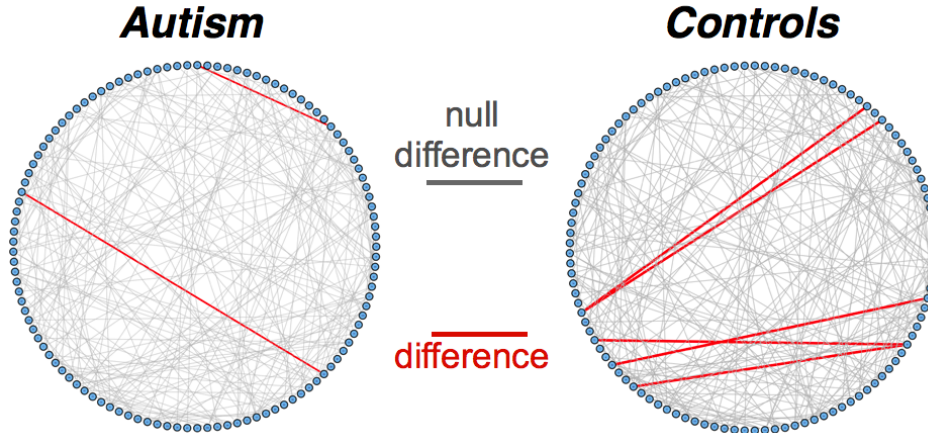


Figure 6: Population Level Differences between Autism and Control Groups.

5.2.  *$R^3$  Data Analysis.* We use  $R^3$  to find differential edges between ASD and control groups. In order to obtain initial estimates of the regularization parameters  $\lambda_i$ , we use StARS with instability parameter  $\beta = .1$  following the procedure in Section 3.1. We then apply  $R^3$  procedure as outlined in Section 3.5. In Figure 6 and Table 2, we report the 7 most differential edges detected by our method. We apply Storey’s direct method (Storey, 2002) to estimate the FDR associated with these discoveries. Notice that the estimated FDR is perhaps larger than expected. This likely occurs because of the limited sample size and large subject heterogeneity. For instance, of the 7 edges we identify, none of them were found to be present in more than 20 individual subject networks in any particular group. Such heterogeneity is

	Group	ROI	ROI	Raw P-value	$\widehat{\text{FDR}}$
1.	Control	Right IFG, po.(27)	Right po. supra-marginal(55)	.0012	.23
2.	Autism	Left frontal pole (16)	Left insula (18)	.0016	.29
3.	Control	Left sup. parietal (50)	Right sup. parietal (51)	.0028	.27
4.	Control	Right IFG, pt(25)	Right posterior supramarginal (55)	.0067	.29
5.	Control	Right post. central (49)	Left superior parietal (50)	.0076	.29
6.	Control	Left lateral occipital cortex(58)	Superior Right fusiform (95)	.0098	.29
7.	Autism	Left Caudate(2)	Left subcallosal cortex (68)	.0102	.29

TABLE 2

We provide a list of top 7 differential edges and report corresponding false discovery rates estimated using Storey’s method.

to be expected in clinical populations (Lenroot and Yeung, 2013). Moreover differences in anatomy and brain parcellation also contribute to this heterogeneity. Nonetheless,  $R^3$  was able to detect marginally significant and biologically relevant edges which could not have been found by mere qualitative inspection of subject networks.

The differential edges we identify align with trends observed in the wider ASD literature (Dichter, 2012; Just et al., 2012; Rudie et al., 2012b; Vissers, X Cohen and Geurts, 2012). Overall, our results support three general patterns that consistently describe the Autistic brain: increased local connectivity, decreased connectivity between the two hemispheres, and decreased activity in inferior frontal gyri (IFG) and fusiform cortex. We summarize specific differential edges and their relevance for ASD below:

- *Differential edges 2,7.* In connectivity studies, ASD networks are characterized by increased short-range connections that connect proximate brain areas (Dichter, 2012; Rudie et al., 2012a), and a noticeable absence of anterior-posterior connections (Just et al., 2012; Vissers, X Cohen and Geurts, 2012), while controls have more frequent long-range connections. The two edges that are more present in our ASD cohort connect regions that are physically close to one another and located in the same hemisphere.
- *Differential edges 4, 6, 7.* In contrast, 3 of the 5 edges that are more present in controls, connect distant brain regions that are located in opposite hemispheres. This supports previous reports of enhanced local connectivity and laterality in ASD subjects, a feature so common in ASD networks that it is anecdotally used as a benchmark for confirming diagnoses.
- *Differential edges 3,5.* Another hallmark of ASD neuroimaging studies is a noticeable absence of activity in the inferior frontal gyrus (IFG). The IFG is a primary component of the mirror neuron network, a network that is often less active in ASDs compared to controls when observing or imitating human activity (Leslie, Johnson-Frey and Grafton, 2004; Iacoboni, 2009). Our data support this finding by showing two of the five edges more present in controls and absent from ASD subjects connecting the IFG to areas in the parietal lobe.
- *Differential edge 6.* Hypoactivity in the fusiform gyrus is another common finding in

ASD subjects compared to controls (Corbett et al., 2009; Pierce and Redcay, 2008). Our results suggest an edge between the right fusiform gyrus and the left lateral occipital cortex that does not occur in ASD.

Our results corroborate a number of common trends in the ASD neuroimaging literature. However, since this is the first study to specifically investigate differential functional connections in ASD, we cannot validate the biological significance of edges we identified using existing literature. We plan to verify these findings using ABIDE data from alternative sites as well as other independent ASD datasets.

**6. Discussion.** In this paper, we have studied a new statistical problem that arises when conducting inference for multi-subject functional connectivity. Our problem assumes a two-level model where subject data arises from a Gaussian graphical model and the edge support is governed by a group level probability, with inference conducted on these group level parameters. This leads to a completely new class of statistical problems that we term Population Post Selection Inference (popPSI). In this paper, we have discussed some of the challenges of our popPSI problem and proposed a new procedure that partially solves these challenges. As we work with a new class of inference problems, however, there are many remaining questions and open areas of related research.

Our model and inference problem is similar in spirit to testing for differences in the elements of two covariance or inverse covariance matrices (Cai, Liu and Xia, 2013). If we let  $\pi^A$  and  $\pi^B$  only take values in  $\{0, 1\}$ , then in fact our problem perfectly coincides with that of Zhao, Cai and Li (2014). Given this, some may argue that we needlessly complicate the problem and potentially lose statistical power by using separate estimators for subject-level networks instead of a joint group estimator. While this would certainly be true in the case where subjects within a group all follow the same distribution, there are a number of reasons why our approach is advantageous for real fMRI data: (1) Assuming that each subject follows a potentially different brain network model mimics assumptions for functional connectivity where neuroscientists expect each subject to have a slightly different brain network; this is especially true for resting-state data in which passive subjects may be thinking about different items. (2) Our models and methods are more closely aligned with the goal of neuroscientists who along with inference wish to examine each subject’s brain network and understand the network differences between subjects both within a group and between groups. Estimating group networks does not permit this analysis across subjects. Most importantly, since group networks do not model between-subject variability, corresponding inferential results do not generalize to larger populations. (3) Our approach is also more robust to potential outliers and artifacts common in neuroimaging (Smith et al., 2011; Power et al., 2012). If a few subjects have gross artifacts or head motion, these can easily corrupt group-level graph estimation and hence group-level inference. By estimating separate graphs for each subject and testing the stability proportion of each edge, our procedure will be more robust to subject-level artifacts. (4) Our framework can easily be extended beyond the two-group model to testing parameters for multiple groups or even for continuous clinical outcomes by using linear and generalized linear mixed effects models and test statistics (Searle, Casella and McCulloch, 2009). This is possible as we directly estimate separate subject networks and the between and within network variability; testing group-level parameters directly cannot easily be extended in this manner. Finally, as our approach can be seen as building upon the standard approach in neuroimaging by incorporating resampling, random effects, and ran-

dom penalization, it is more likely to be adopted by neuroimagers than a new and unfamiliar paradigm.

This paper has focused on characterizing our particular popPSI problem, providing intuition as to why standard approaches in neuroimaging fail, and suggesting a methodological solution. Studying this problem from a theoretical perspective is beyond the scope of this paper and hence, many open theoretical questions remain. We seek to control the overall error rate or FDR of the procedure; studying if this is achievable and under what theoretical conditions is an important open problem. Based on our empirical investigations in Section 4 and our discussion in Section 2.3, we conjecture that this is possible under extensions of an irrepresentable or incoherence condition. More specifically, these conditions limit the correlation between edges that are common across subjects and those that have differential edge probabilities, especially when such common and differential edges belong to the same connected component, as well as limit correlations between those that have differential edge probabilities and the non-edges. Another interesting line of theoretical investigation is relating the overall error rate of the inferential procedure to that of the error rate for graph selection at the subject level. Additionally, there are likely many interesting theoretical questions that arise from characterizing and studying popPSI problems more generally beyond our specific model.

Our model and methods can be extended well beyond testing for the differential presence of an edge in a population of Gaussian graphical models. In particular, our basic approach is applicable to inference for any support related metric such as overall network sparsity or the degree of each node. Here, one could assume the group level parameters follow a Poisson or normal distribution and adjust our random effects Beta-Binomial estimators and test statistics accordingly. Also as mentioned above, we can extend our framework to test multiple groups or continuous clinical outcomes by using linear and generalized linear mixed effects models. Further, other network models such as a sparse covariance model could be used for the subject networks.

For application to multi-subject fMRI data, there are also many other considerations and items to investigate. In Section 1, we mentioned that data for each subject must be parcellated into a matrix of brain regions by time series. More investigations are needed to determine which parcellation method to use and how this affects network estimation and group-level inference. Additionally, many have noted that resting state fMRI data is particularly sensitive to physiological artifacts such as head motion ([Power et al., 2012](#)); further studies are also needed to determine how head motion affects group-level network inference. Finally we note, that our inference paradigm can additionally be employed for task related fMRI experiments as well as in [Tomson et al. \(2013\)](#).

While we introduce a new class of statistical problems, Population PSI, these problems actually arise often in neuroimaging. First, the problems and challenges we outline for the standard approach used for functional connectivity with fMRI data extend to many other forms of connectivity in neuroimaging. Consider structural connectivity which estimates networks based on the number of tracts connecting different brain regions. These tracts, however, are estimated by complicated probabilistic tractography algorithms ([Ciccarelli et al., 2003](#)) from diffusion tensor imaging. Hence, estimates of subject-level networks are imperfect, resulting in two-levels of network variability and then a popPSI-type group level inference problem. Similar problems arise for vector autoregressive graphical models or effective connectivity estimated from EEG, MEG, fMRI, or ECoG data. Additionally, popPSI problems arise in neuroimaging applications beyond network inference where a selection based statistical

learning procedure is applied at the subject level but inference is to be conducted across subjects. Finally, our work provides a cautionary tale about conducting inference on estimated parameters without properly accounting for multiple levels of variability.

In conclusion, we have studied a new problem arising in inference for multi-subject connectivity. As with any new framework many open questions and directions for future research remain. Software for our  $R^3$  procedure will be available as part of the Markov Network Matlab Toolbox <https://bitbucket.org/gastats/monet>.

**Acknowledgments.** M.N. and G.A. are supported by NSF DMS 1209017 and 1264058; S.T. is supported by an NIH training grant 5T32NS048004-08; M.N. is supported by Amazon Web Services (AWS) research grant for computational resources.

#### SUPPLEMENTARY MATERIAL

**Supplement A: Supplementary Material to *Two Sample Inference for Populations of Graphical Models, with Applications to Functional Brain Connectivity*** (doi: [arxiv.org/abs/0000.0000](https://arxiv.org/abs/0000.0000)). Additional simulations demonstrate that  $R^3$  outperforms the standard approach in high dimensional regimes and when increasing differential or common graph density.

#### References.

- ACHARD, S., SALVADOR, R., WHITCHER, B., SUCKLING, J. and BULLMORE, E. (2006). A resilient, low-frequency, small-world human brain functional network with highly connected association cortical hubs. *J. Neurosci.* **26** 63–72.
- BACH, F. R. (2008). Bolasso: model consistent lasso estimation through the bootstrap. In *Proceedings of the 25th International Conference on Machine learning* 33–40. ACM.
- BALACHANDRAN, P., AIROLDI, E. and KOLACZYK, E. (2013). Inference of Network Summary Statistics Through Network Denoising. *arXiv preprint arXiv:1310.0423*.
- BECKMANN, C. F., JENKINSON, M. and SMITH, S. M. (2003). General multilevel linear modeling for group analysis in FMRI. *Neuroimage* **20** 1052–1063.
- BENJAMINI, Y. and YEKUTIELI, D. (2001). The control of the false discovery rate in multiple testing under dependency. *Ann. Statist.* **29** 1165–1188. [MR1869245 \(2002i:62135\)](https://pubmed.ncbi.nlm.nih.gov/11869245/)
- BERK, R., BROWN, L., BUJA, A., ZHANG, K. and ZHAO, L. (2013). Valid post-selection inference. *Ann. Stat.*
- BICKEL, P. J., GÖTZE, F. and VAN ZWET, W. R. (2012). *Resampling fewer than  $n$  observations: gains, losses, and remedies for losses*. Springer.
- BREIMAN, L. (1996). Heuristics of instability and stabilization in model selection. *The annals of statistics* **24** 2350–2383.
- BÜHLMANN, P. L., VAN DE GEER, S. A. and VAN DE GEER, S. (2011). *Statistics for high-dimensional data*. Springer.
- BULLMORE, E. (2012). Functional network endophenotypes of psychotic disorders. *Biol. Psychiatry* **71** 844.
- BULLMORE, E. and SPORNS, O. (2009). Complex brain networks: graph theoretical analysis of structural and functional systems. *Nat Rev Neurosci* **10** 186–198.
- CAI, T., LIU, W. and LUO, X. (2011). A constrained  $\ell_1$  minimization approach to sparse precision matrix estimation. *JASA* **106** 594–607.
- CAI, T., LIU, W. and XIA, Y. (2013). Two-sample covariance matrix testing and support recovery in high-dimensional and sparse settings. *JASA* **108** 265–277.

- CICCARELLI, O., PARKER, G., TOOSY, A., WHEELER-KINGSHOTT, C., BARKER, G., BOULBY, P., MILLER, D. and THOMPSON, A. (2003). From diffusion tractography to quantitative white matter tract measures: a reproducibility study. *Neuroimage* **18** 348–359.
- CORBETT, B. A., CARMEAN, V., RAVIZZA, S., WENDELKEN, C., HENRY, M. L., CARTER, C. and RIVERA, S. M. (2009). A functional and structural study of emotion and face processing in children with autism. *Psychiatry Research: Neuroimaging* **173** 196–205.
- CRADDOCK, R. C., JBABDI, S., YAN, C.-G., VOGELSTEIN, J. T., CASTELLANOS, F. X., DI MARTINO, A., KELLY, C., HEBERLEIN, K., COLCOMBE, S. and MILHAM, M. P. (2013). Imaging human connectomes at the macroscale. *Nature Methods* **10** 524–539.
- CROWDER, M. J. (1978). Beta-binomial Anova for proportions. *Applied Statistics* 34–37.
- DANAHER, P., WANG, P. and WITTEN, D. M. (2011). The joint graphical lasso for inverse covariance estimation across multiple classes. *arXiv preprint arXiv:1111.0324*.
- D’ASPREMONT, A., BANERJEE, O. and EL GHAOU, L. (2006). First-order methods for sparse covariance selection. *ArXiv Mathematics e-prints*.
- DICHTER, G. S. (2012). Functional magnetic resonance imaging of autism spectrum disorders. *Dialogues in clinical neuroscience* **14** 319.
- EFRON, B. and TIBSHIRANI, R. J. (1993). *An Introduction to the Bootstrap*. Chapman & Hall, London, U.K.
- FISCHL, B., VAN DER KOUWE, A., DESTRIEUX, C., HALGREN, E., SÉGONNE, F., SALAT, D. H., BUSA, E., SEIDMAN, L. J., GOLDSTEIN, J., KENNEDY, D. et al. (2004). Automatically parcellating the human cerebral cortex. *Cerebral cortex* **14** 11–22.
- FRIEDMAN, J., HASTIE, T. and TIBSHIRANI, R. J. (2008). Sparse inverse covariance estimation with the graphical lasso. *Biostatistics* **9** 432–441.
- GUO, J., ELIZAVETA LEVINA, G. M. and ZHU, J. (2011). Joint Estimation of Multiple Graphical Models. *Biometrika* **98** 1–15.
- HSIEH, C.-J., SUSTIK, I. MÁTYÁS A. AND DHILLON and RAVIKUMAR, P. (2011). Sparse Inverse Covariance Matrix Estimation Using Quadratic Approximation. In *Advances in Neural Information Processing Systems 24* (J. Shawe-Taylor, R. S. Zemel, P. Bartlett, F. C. N. Pereira and K. Q. Weinberger, eds.) 2330–2338.
- HUANG, S., LI, J., SUN, L., YE, J., FLEISHER, A., WU, T., CHEN, K. and REIMAN, E. (2010). Learning brain connectivity of Alzheimer’s disease by sparse inverse covariance estimation. *NeuroImage* **50** 935–949.
- IACOBONI, M. (2009). Imitation, empathy, and mirror neurons. *Annual review of psychology* **60** 653–670.
- INDI (2013). ABIDE: Autism Brain Imaging Data Exchange.
- JANSSEN, A. (1997). Studentized permutation tests for non-i.i.d. hypotheses and the generalized Behrens-Fisher problem. *Statistics & Probability Letters* **36** 9–21.
- JAVANMARD, A. and MONTANARI, A. (2013). Confidence Intervals and Hypothesis Testing for High-Dimensional Regression. *arXiv preprint arXiv:1306.3171*.
- JUST, M. A., KELLER, T. A., MALAVE, V. L., KANA, R. K. and VARMA, S. (2012). Autism as a neural systems disorder: a theory of frontal-posterior underconnectivity. *Neuroscience & Biobehavioral Reviews* **36** 1292–1313.
- KLEINMAN, J. C. (1973). Proportions with extraneous variance: single and independent samples. *JASA* **68** 46–54.
- LEE, S., SHIMOJO, S. and O’DOHERTY, J. (2014). Neural computations underlying arbitration between model-based and model-free learning. *Neuron* **81** 687–699.

- LENROOT, R. K. and YEUNG, P. K. (2013). Heterogeneity within autism spectrum disorders: what have we learned from neuroimaging studies? *Front. Hum. Neurosci.* **7**.
- LESLIE, K. R., JOHNSON-FREY, S. H. and GRAFTON, S. T. (2004). Functional imaging of face and hand imitation: towards a motor theory of empathy. *Neuroimage* **21** 601–607.
- LI, S., HSU, L., PENG, J. and WANG, P. (2011). Bootstrap inference for network construction. *arXiv preprint arXiv:1111.5028*.
- LIANG, K.-Y. and HANFELT, J. (1994). On the use of the quasi-likelihood method in teratological experiments. *Biometrics* **50** 872–880.
- LIANG, K.-Y. and SELF, S. G. (1996). On the asymptotic behaviour of the pseudolikelihood ratio test statistic. *J. Roy. Statist. Soc. Ser. B* 785–796.
- LIU, H., ROEDER, K. and WASSERMAN, L. (2010). Stability Approach to Regularization Selection (StARS) for High Dimensional Graphical Models In *Advances in Neural Information Processing Systems*.
- MARRELEC, G., KRAINIK, A., DUFFAU, H., PÉLÉGRINI-ISSAC, M., LEHÉRICY, S., DOYON, J. and BENALI, H. (2006). Partial correlation for functional brain interactivity investigation in functional MRI. *Neuroimage* **32** 228–237.
- MEDA, S. A., GILL, A., STEVENS, M. C., LORENZONI, R. P., GLAHN, D. C., CALHOUN, V. D., SWEENEY, J. A., TAMMINGA, C. A., KESHAVAN, M. S., THAKER, G. et al. (2012). Differences in resting-state functional magnetic resonance imaging functional network connectivity between schizophrenia and psychotic bipolar probands and their unaffected first-degree relatives. *Biological psychiatry* **71** 881–889.
- MEINSHAUSEN, N. (2008). A note on the Lasso for Gaussian graphical model selection. *Statistics & Probability Letters* **78** 880–884.
- MEINSHAUSEN, N. and BÜHLMANN, P. (2006). High-dimensional graphs and variable selection with the lasso. *Ann. Stat.* **34** 1436–1462.
- MEINSHAUSEN, N. and BUHLMANN, P. (2010). Stability selection. *J. Roy. Statist. Soc. Ser. B* **72** 417–473.
- MILHAM, M. P. (2012). Open neuroscience solutions for the connectome-wide association era. *Neuron* **73** 214–218.
- MILHAM, M. P., FAIR, D., MENNES, M. and MOSTOFKY, S. H. (2012). The ADHD-200 consortium: a model to advance the translational potential of neuroimaging in clinical neuroscience. *Front. Sys. Neurosci.* **6** 62.
- MOORE, D. F. (1986). Asymptotic properties of moment estimators for overdispersed counts and proportions. *Biometrika* **73** 583–588.
- NARAYAN, M., ALLEN, G. I. and TOMSON, S. (2015a). Supplement to Two Sample Inference for Populations of Graphical Models with Applications to Functional Brain Connectivity. (*Preprint*).
- NARAYAN, M., ALLEN, G. I. and TOMSON, S. (2015b). Two Sample Inference for Populations of Graphical Models with Applications to Functional Brain Connectivity. (*Preprint*).
- NICHOLS, T. E. and HOLMES, A. P. (2002). Nonparametric permutation tests for functional neuroimaging: a primer with examples. *Human brain mapping* **15** 1–25.
- NIELSEN, J. A., ZIELINSKI, B. A., FLETCHER, P. T., ALEXANDER, A. L., LANGE, N., BIGLER, E. D., LAINHART, J. E. and ANDERSON, J. S. (2013). Multisite functional connectivity MRI classification of autism: ABIDE results. *Front. Hum. Neurosci.* **7** 599.
- PALANIYAPPAN, L., SIMMONITE, M., WHITE, T. P., LIDDLE, E. B. and LIDDLE, P. F. (2013). Neural Primacy of the Salience Processing System in Schizophrenia. *Neuron* **79** 814–828.
- PIERCE, K. and REDCAY, E. (2008). Fusiform function in children with an autism spectrum

- disorder is a matter of “who”. *Biological psychiatry* **64** 552–560.
- POWER, J. D., COHEN, A. L., NELSON, S. M., WIG, G. S., BARNES, K. A., CHURCH, J. A., VOGEL, A. C., LAUMANN, T. O., MIEZIN, F. M., SCHLAGGAR, B. L. et al. (2011). Functional network organization of the human brain. *Neuron* **72** 665–678.
- POWER, J. D., BARNES, K. A., SNYDER, A. Z., SCHLAGGAR, B. L. and PETERSEN, S. E. (2012). Spurious but systematic correlations in functional connectivity MRI networks arise from subject motion. *Neuroimage* **59** 2142–2154.
- RAVIKUMAR, P., WAINWRIGHT, M. J., RASKUTTI, G. and YU, B. (2011). High-dimensional covariance estimation by minimizing  $\ell_1$ -penalized log-determinant divergence. *Electronic Journal of Statistics* **5** 935–980.
- REN, Z., SUN, T., ZHANG, C.-H. and ZHOU, H. H. (2013). Asymptotic normality and optimality in estimation of large Gaussian graphical model. *arXiv preprint arXiv:1309.6024*.
- RIDOUT, M. S., DEMÉTRIO, C. G. B. and FIRTH, D. (1999). Estimating Intraclass Correlation for Binary Data. *Biometrics* **55** pp. 137-148.
- ROTHMAN, A. J., BICKEL, P. J., LEVINA, E., ZHU, J. et al. (2008). Sparse permutation invariant covariance estimation. *Electronic Journal of Statistics* **2** 494–515.
- RUBINOV, M. and SPORNS, O. (2010). Complex network measures of brain connectivity: uses and interpretations. *Neuroimage* **52** 1059–1069.
- RUDIE, J., BROWN, J., BECK-PANCER, D., HERNANDEZ, L., DENNIS, E., THOMPSON, P., BOOKHEIMER, S. and DAPRETTO, M. (2012a). Altered Functional and Structural Brain Network Organization in Autism. *NeuroImage: Clinical*.
- RUDIE, J. D., SHEHZAD, Z., HERNANDEZ, L. M., COLICH, N. L., BOOKHEIMER, S. Y., IACOBONI, M. and DAPRETTO, M. (2012b). Reduced functional integration and segregation of distributed neural systems underlying social and emotional information processing in autism spectrum disorders. *Cerebral Cortex* **22** 1025–1037.
- RYALI, S., CHEN, T., SUPEKAR, K. and MENON, V. (2012). Estimation of functional connectivity in fMRI data using stability selection-based sparse partial correlation with elastic net penalty. *NeuroImage* **59** 3852–3861.
- SEARLE, S. R., CASELLA, G. and MCCULLOCH, C. E. (2009). *Variance components* **391**. Wiley-Interscience.
- SHAH, R. D. and SAMWORTH, R. J. (2013). Variable selection with error control: another look at stability selection. *J. Roy. Statist. Soc. Ser. B* **75** 55–80.
- SIMPSON, S. L., BOWMAN, F. D., LAURIENTI, P. J. et al. (2013a). Analyzing complex functional brain networks: fusing statistics and network science to understand the brain. *Statistics Surveys* **7** 1–36.
- SIMPSON, S. L., LYDAY, R. G., HAYASAKA, S., MARSH, A. P. and LAURIENTI, P. J. (2013b). A permutation testing framework to compare groups of brain networks. *Front. Comput. Neurosci.* **7**.
- SMITH, S. M. (2012). The future of FMRI connectivity. *NeuroImage* **0** -.
- SMITH, S. M., MILLER, K. L., SALIMI-KHORSHIDI, G., WEBSTER, M., BECKMANN, C. F., NICHOLS, T. E., RAMSEY, J. D. and WOOLRICH, M. W. (2011). Network modelling methods for FMRI. *NeuroImage* **54** 875–891.
- SMITH, S. M., VIDAURRE, D., BECKMANN, C. F., GLASSER, M. F., JENKINSON, M., MILLER, K. L., NICHOLS, T. E., ROBINSON, E. C., SALIMI-KHORSHIDI, G., WOOLRICH, M. W. et al. (2013). Functional connectomics from resting-state fMRI. *Trends Cogn. Sci.* **17** 666–682.
- SPORNS, O. (2011). The Non-Random Brain: efficiency, economy and complex dynamics.

- Front. Comput. Neurosci.* **5**.
- STOREY, J. D. (2002). A direct approach to false discovery rates. *J. Roy. Statist. Soc. Ser. B* **64** 479–498.
- TAM, A., ORBAN, P., DANSEREAU, C., BELLEVILLE, S., BENOIT, S., DAGHER, A., JOUBERT, S., MONCHI, O., PETERS, F., ROSA-NETO, P. et al. (2014). Connectome-wide analysis of differences between normal aging, mild cognitive impairment, and dementia of the Alzheimer’s type using resting-state fMRI connectivity. *Alzheimer’s & Dementia: The Journal of the Alzheimer’s Association* **10** P827–P828.
- TAO, H., GUO, S., GE, T., KENDRICK, K. M., XUE, Z., LIU, Z. and FENG, J. (2013). Depression uncouples brain hate circuit. *Mol Psychiatry* **18** 101–111.
- TOMSON, S. N., NARAYAN, M., ALLEN, G. I. and EAGLEMAN, D. M. (2013). Neural Networks of Colored Sequence Synesthesia. *J. Neurosci.* **33** 14098–14106.
- TURK-BROWNE, N. B. (2013). Functional interactions as big data in the human brain. *science* **342** 580–584.
- VAN DE GEER, S., BÜHLMANN, P. and RITOV, Y. (2013). On asymptotically optimal confidence regions and tests for high-dimensional models. *arXiv preprint arXiv:1303.0518*.
- VAROQUAUX, G. and CRADDOCK, R. C. (2013). Learning and comparing functional connectomes across subjects. *NeuroImage*.
- VISSERS, M. E., X COHEN, M. and GEURTS, H. M. (2012). Brain connectivity and high functioning autism: a promising path of research that needs refined models, methodological convergence, and stronger behavioral links. *Neuroscience & Biobehavioral Reviews* **36** 604–625.
- VOGELSTEIN, J. T., RONCAL, W. G., VOGELSTEIN, R. J. and PRIEBE, C. E. (2013). Graph Classification Using Signal-Subgraphs: Applications in Statistical Connectomics. *IEEE Trans. Pattern Anal. Mach. Intell.* **35** 1539–1551.
- WANG, J.-H., ZUO, X., GOHEL, S., MILHAM, M. P., BISWAL, B. B. and HE, Y. (2011). Graph theoretical analysis of functional brain networks: test-retest evaluation on short-and long-term resting-state functional MRI data. *PloS one* **6** e21976.
- WASSERMAN, L., KOLAR, M. and RINALDO, A. (2013). Estimating undirected graphs under weak assumptions. *arXiv preprint arXiv:1309.6933*.
- WASSERMAN, L. and ROEDER, K. (2009). High dimensional variable selection. *Ann. Stat.* **37** 2178.
- WEIL, C. (1970). Selection of the valid number of sampling units and a consideration of their combination in toxicological studies involving reproduction, teratogenesis or carcinogenesis. *Food and cosmetics toxicology* **8** 177–182.
- WORSLEY, K. J., LIAO, C., ASTON, J., PETRE, V., DUNCAN, G., MORALES, F. and EVANS, A. (2002). A general statistical analysis for fMRI data. *Neuroimage* **15** 1–15.
- YAN, C.-G., CHEUNG, B., KELLY, C., COLCOMBE, S., CRADDOCK, R. C., DI MARTINO, A., LI, Q., ZUO, X., CASTELLANOS, F. X. and MILHAM, M. P. (2013). A comprehensive assessment of regional variation in the impact of head micromovements on functional connectomics. *Neuroimage* **76** 183–201.
- ZALESKY, A., FORNITO, A. and BULLMORE, E. T. (2010). Network-based statistic: identifying differences in brain networks. *Neuroimage* **53** 1197–1207.
- ZALESKY, A., COCCHI, L., FORNITO, A., MURRAY, M. M. and BULLMORE, E. (2012). Connectivity differences in brain networks. *Neuroimage*.
- ZHANG, C.-H. and ZHANG, S. S. (2014). Confidence intervals for low dimensional parameters in high dimensional linear models. *J. Roy. Statist. Soc. Ser. B* **76** 217–242.

- ZHAO, S. D., CAI, T. T. and LI, H. (2014). Direct estimation of differential networks. *Biometrika* **101** 253–268.
- ZHAO, P. and YU, B. (2006). On model selection consistency of Lasso. *The Journal of Machine Learning Research* **7** 2541–2563.

## APPENDIX A: ADDITIONAL FIGURES AND SIMULATION STUDIES

We present additional figures and simulation studies that complement those in [Narayan, Allen and Tomson \(2015b\)](#). First in Figure [A.7](#), we present confusion adjacency matrices for specific examples from our Simulation Study described in [Narayan, Allen and Tomson \(2015b\)](#) and corresponding to Figure 4 and Table 1. These illustrate the location of false positive and false negative edges for group inference with the lower-triangular portion showing the true common and differential edges and the upper-triangular portion showing the rejected edges that are declared differential. Overall, we can see that  $R^3$  offers substantial improvements over the standard method which has both high Type I and Type II error rates. Notice also, that false positives where common edges are mistaken as differential edges are far more likely to occur when graph selection errors are more severe. These are either (i) when differential edges are highly correlated as in Case I scenarios where the differential edges are clustered, or (ii) when the differential and common edges are highly connected as in small world or hub graphs.

Next, we study how changing the number of differential and common edges in the network structure affects our method and the standard approach. In Figures [A.8](#) and [A.9](#), we present ROC curves as the number of differential edges is increased and the number and degree of common edges are increased respectively. Other than these described changes, simulation scenarios are as described in [Narayan, Allen and Tomson \(2015b\)](#). Increasing the number of differential edges results in a slight loss of statistical power. Increasing the number and average degree of common edge support in the network structure, on the other hand, can result in severe loss of statistical power. Here, dense graph structures for highly connected graph types are known to lead to high graph selection error rates which in turn severely bias our test statistics, resulting in increased Type I and Type II errors. These results are also born out in the accompanying Tables [A.3](#) and [A.4](#) which give the average true positive rate and false discovery portion for the rejected tests.

Finally, we present a high-dimensional simulation study in Figure [A.10](#) and Table [A.5](#) that complements Figure 4 and Table 1 in [Narayan, Allen and Tomson \(2015b\)](#). For this simulation, we let  $p = 100 > T = 80$  and all other parameters are as described in [Narayan, Allen and Tomson \(2015b\)](#). Trends observed in the lower-dimensional case are also observed here. Interestingly, this simulation comparatively shows a slight increase in statistical power with lower estimated false positive rates. This likely occurs as the number of differential edges is fewer relative to  $p$  and hence networks are less dense resulting in fewer graph selection errors.

Overall, these simulations reveal that  $R^3$  continues to perform well in a variety of settings. Combining these findings with investigations in [Narayan, Allen and Tomson \(2015b\)](#), we see that  $R^3$  is most affected by graph selection errors that occur for highly dense and correlated network structures.

Case	Sim Type	Metric	$R^3,  D  = 100$	St., $ D  = 100$	$R^3,  D  = 200$	St., $ D  = 200$
II	SmallW	TPR	0.836 (0.092)	0.323 (0.125)	0.790 (0.088)	0.250 (0.065)
		FDP	0.264 (0.059)	0.798 (0.042)	0.211 (0.047)	0.711 (0.028)
II	Banded	TPR	0.871 (0.062)	0.362 (0.104)	0.855 (0.068)	0.311 (0.100)
		FDP	0.273 (0.068)	0.767 (0.029)	0.166 (0.046)	0.654 (0.045)
II	Hub	TPR	0.972 (0.028)	0.540 (0.166)	0.956 (0.026)	0.518 (0.094)
		FDP	0.038 (0.026)	0.613 (0.066)	0.040 (0.013)	0.446 (0.033)

TABLE A.3

Increasing the Number of Differential Edges. Average true positive rate (TPR) and false discovery proportion (FDP) for tests rejected by  $R^3$  and the standard approach when controlling the FDR at 10% via the Benjamini-Yekutieli method; standard errors are given in parentheses. Both approaches show a mild loss of statistical power as the number of differential edges increases.

Case	Sim Type	Metric	$R^3, \text{Deg} = 5$	St., $\text{Deg} = 5$	$R^3, \text{Deg} = 15$	St., $\text{Deg} = 15$
II	SmallW	TPR	0.811 (0.071)	0.295 (0.115)	0.157 (0.055)	0.235 (0.038)
		FDP	0.230 (0.095)	0.724 (0.061)	0.613 (0.044)	0.866 (0.022)
II	Banded	TPR	0.932 (0.055)	0.443 (0.105)	0.884 (0.057)	0.361 (0.066)
		FDP	0.158 (0.059)	0.653 (0.035)	0.193 (0.081)	0.668 (0.040)
II	Hub	TPR	0.956 (0.039)	0.516 (0.151)	0.572 (0.155)	0.251 (0.091)
		FDP	0.054 (0.038)	0.513 (0.074)	0.744 (0.049)	0.809 (0.030)

TABLE A.4

Increasing the Number of Common Edges and Common Network Degree. Average true positive rate (TPR) and false discovery proportion (FDP) for tests rejected by  $R^3$  and the standard approach when controlling the FDR at 10% via the Benjamini-Yekutieli method; standard errors are given in parentheses. As expected, both methods have a severe loss of statistical power as the graph density increases and hence graph selection errors increase for highly-connected small world and hub graphs.

Case	Sim Type	Metric	$R^3$	Standard Test	$R^2 = (RS, RE)$	$R^2 = (RS, RP)$
I	SmallW	TPR	0.959 (0.019)	0.770 (0.068)	0.915 (0.037)	0.961 (0.019)
		FDP	0.131 (0.048)	0.606 (0.019)	0.200 (0.053)	0.612 (0.012)
I	Banded	TPR	0.968 (0.017)	0.786 (0.073)	0.922 (0.038)	0.970 (0.016)
		FDP	0.151 (0.070)	0.565 (0.025)	0.222 (0.063)	0.585 (0.023)
I	Hub	TPR	0.979 (0.014)	0.880 (0.065)	0.946 (0.032)	0.981 (0.014)
		FDP	0.185 (0.146)	0.522 (0.039)	0.230 (0.086)	0.567 (0.078)
Case	Sim Type	Metric	$R^3$	Standard Test	$R^2 = (RS, RE)$	$R^2 = (RS, RP)$
II	SmallW	TPR	0.960 (0.016)	0.761 (0.056)	0.930 (0.023)	0.964 (0.016)
		FDP	0.046 (0.019)	0.492 (0.017)	0.078 (0.021)	0.506 (0.011)
II	Banded	TPR	0.962 (0.012)	0.757 (0.081)	0.930 (0.033)	0.967 (0.014)
		FDP	0.056 (0.044)	0.462 (0.025)	0.087 (0.055)	0.489 (0.033)
II	Hub	TPR	0.974 (0.014)	0.803 (0.057)	0.946 (0.023)	0.976 (0.014)
		FDP	0.038 (0.016)	0.396 (0.015)	0.070 (0.021)	0.410 (0.011)

TABLE A.5

High-dimensional results in terms of average true positive rate (TPR) and false discovery proportion (FDP) for tests rejected by each method when controlling the FDR at 10% via the Benjamini-Yekutieli method; standard errors are given in parentheses.

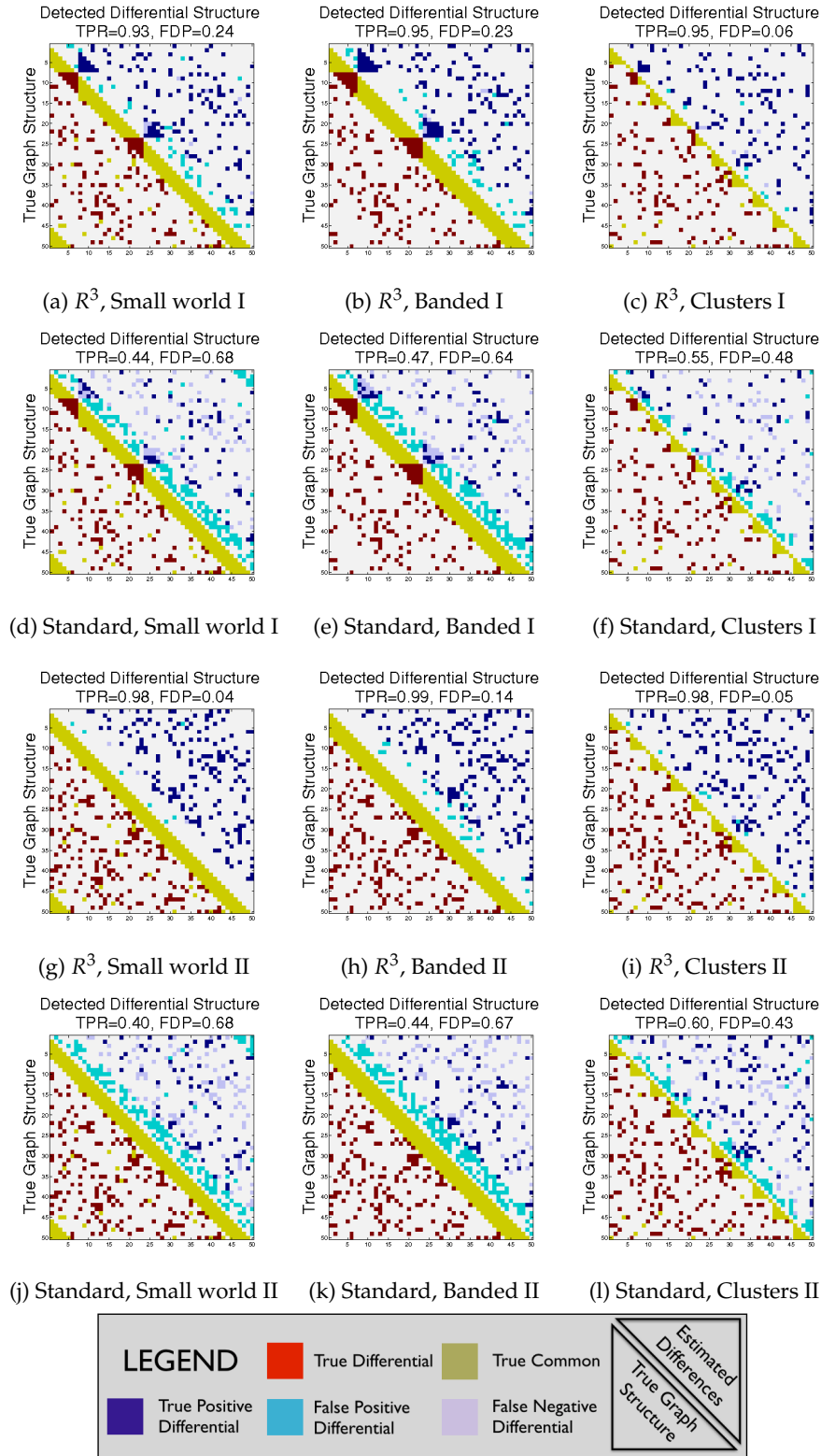


Figure A.7: Confusion adjacency matrices illustrating the location of false positives and false negatives for group-level inference detected by both our  $R^3$  and the standard approach. Each example accompanies one of the six simulation scenarios described in Narayan, Allen and Tomson (2015b).

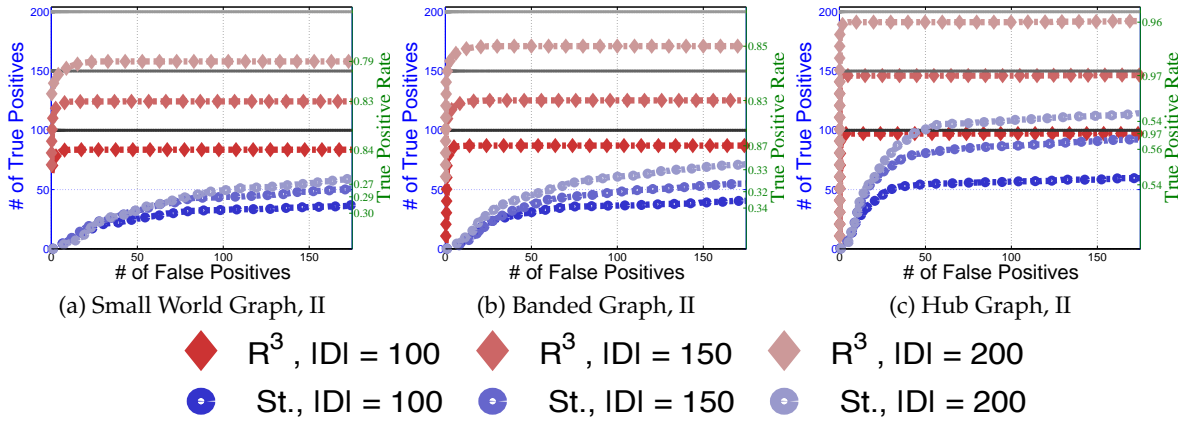


Figure A.8: Increasing the Number of Differential Edges. ROC curves for sequentially rejected tests comparing  $R^3$  to the standard method when the number of differential edges are increased:  $|D| = \{100, 150, 200\}$ ; otherwise the simulation is as described in Narayan, Allen and Tomson (2015b). As the number of differential edges increases, the number of alternative hypotheses also increases; hence, true positive rates for each curve are denoted on the right  $y - axis$ . Here, increases in the number of differential edges result in a mild loss of statistical power.

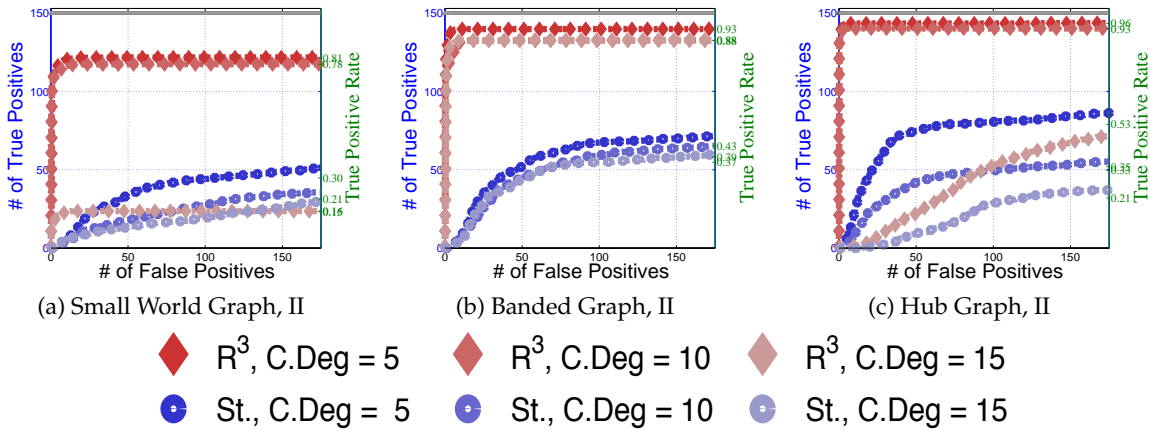


Figure A.9: Increasing the Number of Common Edges and Common Network Degree. ROC curves for sequentially rejected tests comparing  $R^3$  to the standard method when the number of common edges are increased such that the average network degree is equal to 5, 10, or 15; otherwise the simulation is as described in Narayan, Allen and Tomson (2015b). As the common network degree increases, the number of alternative hypotheses also increases accordingly; hence, true positive rates for each curve are denoted on the right  $y - axis$ . Here, increases network degree are known to increase graph selection errors. As a result, statistical power dramatically decreases for networks with high degree.

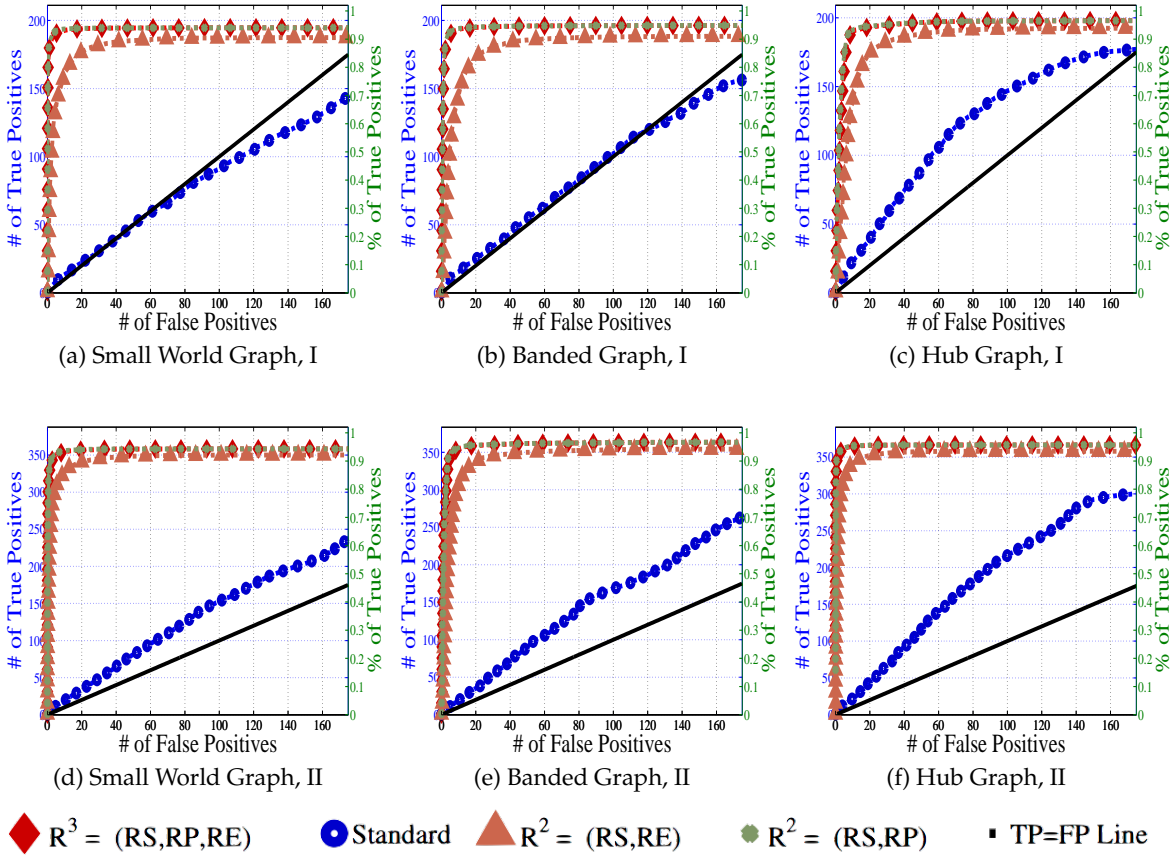


Figure A.10: High-dimensional results in terms of average ROC curves for sequentially rejected tests comparing our method to the standard approach,  $R^2 = (RS, RE)$ , and  $R^2 = (RS, RP)$  for each network structure type and Case I and II type differential edges. Analogously to the lower dimensional case, methods employing random penalization (RP) improve statistical power.